Modelling the poroelastoplastic behaviour of soils subjected to internal erosion by suffusion

Quentin Rousseau, Giulio Sciarra, Rachel Gelet, Didier Marot

Modelling the poroelastoplastic behaviour of soils subjected to internal erosion by suffusion

Quentin Rousseau[1] *, Giulio Sciarra[1], Rachel Gelet[2], Didier Marot[2]

[1]Institut de Recherche en Génie Civil et Mécanique (UMR CNRS 6183), Ecole Centrale de Nantes, Nantes, France

[2] Institut de Recherche en Génie Civil et Mécanique (UMR CNRS 6183), Université de Nantes, Saint-Nazaire, France

* quentin.rousseau@ec-nantes.fr

Abstract: Granular soils subjected to seepage flow may suffer suffusion, i.e. a selective internal erosion. Extending the classical approach of poromechanics, we deduce a new form of the Clausius-Duhem inequality accounting for dissipation due to suffusion and we deduce restrictions on the constitutive laws of the soil. We suggest (*i*) a possible coupling between the seepage forces and the suffusion kinetics (*ii*) an extension of an existing elastoplastic model for the skeleton mechanical behaviour. Numerical integrations of the elastoplastic model are carried out under drained axisymmetric triaxial and oedometric conditions. As a result, we prove that the extended model is able to qualitatively reproduce the suffusion induced strains as well as the strength reduction experimentally observed. Predictions on the oedometric behaviour of suffusive soils are also provided.

Keywords: Suffusion, thermodynamics, poromechanical model

1 Introduction

Seepage flow through a cohesionless granular medium may induce detachment, transport and even interlocking of the grains of the granular skeleton. Detachment corresponds to the loss of contact between a grain and the solid skeleton; transport refers to its convected displacement along the hydraulic flux; interlocking corresponds to the capture of the transported particle by the solid skeleton. Once interlocking occurs the contact between the ripped out fine particles and the solid skeleton is recovered. Internal erosion [1] is the combination of these three processes. When internal erosion is selective (i.e. it concerns the finest fraction of the grains constituting the skeleton) and takes place within the granular assembly, we call it suffusion.
Suffusion initiation and development highly depends on the nature of the soil, which on the one hand must contain fine grains to be detached and transported and on the other hand should be characterized by a sufficiently coarse pore network to let eroded fine grains be transported through a non negligible distance. This means that suffusion does not occur for all grading of soil. Among three types of grain size distributions: linearly graded soils, gap-graded soils and upwardly concave graded soils, the last two were identified as "unstable", i.e. can be affected by suffusion[2, 3]. The shape of the grains also plays an important role in triggering suffusion: for clayey sands with the same grain size distribution, the higher the angularity of coarse grains, the larger the erosion resistance[4].
Even when a soil is expected to be affected by suffusion, a seepage flow is generally thought to be required to trigger and continue the phenomenon. Indeed several studies have explored the link between seepage flow and suffusion initiation and have advocated the existence of a hydraulic threshold for suffusion to

occur. This threshold is generally defined via three different approaches: (*i*) a critical hydraulic gradient[5] (*ii*) a critical hydraulic shear stress[6], or (*iii*) a critical fluid velocity[7]. According to these methods, one can deduce a critical hydraulic threshold for a given set-up, however these approaches do not provide any information about suffusion kinetics. Moreover, the critical hydraulic threshold is subjected to scale effects[8] and depends on the history of hydraulic loading[9]. These conclusions have enlighted the need for a new characterization and classification of suffusion susceptibility, which has recently been proposed based on the energy dissipated by the pore fluid during the suffusion test[10]; this new energy approach has the very good properties of being neither scale-dependent nor affected by the history of hydraulic loading.
From the mechanical point of view, the onset of suffusion has been related not only to variations of local hydraulic gradients but also to the stress state of the soil[11]. Testing gap-graded soils, the effect of the mechanical stress state on the initiation of suffusion has been studied with a modified tri-axial apparatus that allows vertical seepage flows[12]. Due to the decrease of the initial porosity, the critical hydraulic gradient that initiates suffusion increases with the value of the mean effective stress. Moreover, the critical hydraulic gradient tends to increase with the deviatoric stress ratio, until a maximum value is attained; from that point the critical hydraulic gradient begins to decrease. Regarding suffusion development, the increase of the mean effective stress implies the decrease of the rate of eroded mass[13].
Conversely since suffusion involves detachment, transport and interlocking of the fine particles, it also affects the hydraulic behaviour of the soil. Also, the microstructure is widly impacted: changes in both the granulometry distribution and the porosity of the soil are commonly observed[12, 14]. Moreover, the delay between detachment, transport and interlocking, which can potentially occur at different location within the soil mass, increases the heterogeneity of the soil microstructure. In the worst cases, a preferential flow path may appear within the soil[14, 15].
By changing the fine content and therefore the microstructure of the skeleton, suffusion affects also the mechanical properties of the soil. To investigate the role of the fine content on the mechanical properties of the soil, mechanical tests have been performed over reconstituted soils characterized by different amount of fines[16]; the results of these tests can be compared with post-suffusion mechanical tests on eroded sample[17]. The main result is that the mechanical behaviour of a suffusive soil is not the same as that of a reconstituted one having the same fine content. This means that average parameters are not sufficient to characterize the soil microstructure after suffusion, but additional informations concerning the local value of the intergranular void space is mandatory. It has been shown that locally suffusion may induce volumetric strain in the soil, yielding soil settlement[15]. Numerical experiments based on the use of the Discrete Elements Method[18, 19, 20, 21] have provided similar results as those of the above mentioned laboratory tests. Starting from a polydisperse granular medium, the suffusion kinetics has been modelled as a selective particle removal[18, 19], or induced by the seepage flow[20, 21], also in these cases a volumetric strain has been observed. The volumetric strain is due to the state of stress in the vicinity of the detached fine grains: if eroded fine grains are initially parts of the force chains, their detachment induces a loss of equilibrium; in order to make the force chains network balanced again, grain rearrangment occurs which modifies the chain geometry[21]. At the macroscopic scale, this rearrangment causes volumetric strains. Conversely, if eroded grains are initially free of charge, the force chains network is not affected by grain ripping so that no rearrangement and consequently no volumetric strain occurs. A competition between the increase of the specific volume and the contraction as a response of particle removal has been enlighted[18]. This conclusion can be interpreted in term of the signed distance between the soil state and the critical state[18, 19]: if the soil state is above the critical state (which is possible for dense soils), then dilation occurs during suffusion. Conversely, if the soil state is below the critical state, compaction occurs during suffusion. Besides the effect on strain evolution, suffusion affects also the strength of the soil. Several drained triaxial tests have been conduced over dense soils that exhibit initially a dilative and softening behaviour (i.e. soils for which a peak strength exists). The suffusion effect in this case is the loss of density: the suffused soil behaves like a loose soil and the peak strength disappears[17, 20, 19]. Conversely, drained triaxial tests carried out over initially loose samples have shown that the effect of suffusion is mainly the reduction of the residual strength[22].

Implementing within a suitable constitutive model the effects of suffusion on the hydromechanical response of soils as well as vice-versa the effects of hydromechanical loading on suffusion has been, since few years, the subject of significant modelling efforts within the scientific community of continuum geomechanics. The main efforts have been realized in the framework of sand production during hydrocarbons extraction[23, 24, 25, 26, 27, 28]. In this framework, internal erosion kinetics has been accounted for as a mass source into the mass balance equations of the fluid and the solid phases of porous medium, thus resulting into a porosity variation. An additional equation specifying the rate of eroded mass has then been introduced. The effect of erosion on the mechanical response has also been taken into account assuming the corresponding porosity variation as a kind of damage parameter, reducing the elastic stiffness and the internal cohesion of the sandstone[24, 25, 27].
In different contexts, few other constitutive laws aiming at modelling suffusion kinetics in granular soils have been proposed[29, 15]. More recently, the constitutive modelling of soil subjected to internal erosion has been explored using thermodynamics of porous media[30], the internal erosion kinetics being accounted for by a new internal variable: ϕ^{er} the porosity variation induced by internal erosion. In a similar way as in the model proposed by Stavropoulou et al[24]. this porosity variation is regarded as a kind of damage parameter and the rate of erosion is once again assumed to be proportional to the distance between the current and the critical hydraulic shear stress.
With the aim of going deeper into the constitutive modelling of suffusion, our study presents a new approach to model coupling effects between the suffusion process and the hydro-mechanical response of a granular soil. Adopting the framework of classical poromechanics[31], the kinematics of the suffusive soil is established in Section 2. In Section 3, the external working is stated in order to express the fundamental principles of thermodynamics in Section 4. Clausius-Duhem inequality is generalised by considering the solid and the fluid dissipations to be fully coupled because of suffusion and the constitutive prescriptions for the suffusive soil are given in Section 5. In Section 6 an existing elasto-plastic model for soils[32] is extended by introducing the suffusion induced porosity as a hardening variable and a parameter of the characteristic state. In order to reproduce experimental results[17, 22], numerical integrations of the elasto-plastic constitutive model have been carried out in Section 7, for monotonic mechanical loadings, under drained triaxial and oedometric conditions. In this paper, the continuum mechanics sign convention is employed.

2 Kinematics and mass balances

Each of the phases of a porous medium is endowed with its own kinematics and mass content. Accordingly, this section presents the basic defintions and the balances of mass specific to the hydro-mechanical response of a suffusive mixture. The suffusive porous medium is constitued of two phases: a solid and a fluid saturating the porous network. The superscript s refers to the solid phase, including both erodible and non-erodible grains, and the superscript f refers to the fluid phase as a binary mixture, constitued of the pore liquid (denoted by the superscript wf) and fluidized grains (denoted by the superscript pf).
Let $\mathcal{D}_0$ be the reference configuration of the solid skeleton, $\mathcal{T}$ a time interval and $\mathcal{E}$ the Euclidian space of positions, then $\boldsymbol{\chi} : \mathcal{D}_0 \times \mathcal{T} \to \mathcal{E}$ indicates the placement map of the solid skeleton. The image $\mathcal{D}$ of the reference configuration $\mathcal{D}_0$ under $\boldsymbol{\chi}$ denotes the current configuration of the porous medium and it is a part of $\mathcal{E}$. Let $\boldsymbol{X} \in \mathcal{D}_0$ be the reference position of a solid material particle and $\boldsymbol{x}$ its placement in the current configuration then: $\boldsymbol{x} = \boldsymbol{\chi}(\boldsymbol{X}, t)$. By time-differentiating $\boldsymbol{\chi}$, we introduce the velocity $\boldsymbol{v}^s$ of the skeleton and the related particle accelation $\boldsymbol{\gamma}^s$:

$$\boldsymbol{v}^s = \frac{d\boldsymbol{\chi}}{dt} \quad \text{and} \quad \boldsymbol{\gamma}^s = \frac{d^s\boldsymbol{v}^s}{dt} \tag{1}$$

In equation (1) and in the following d^s/dt indicates the time derivative following the motion of a solid

material particle. We denote by $\boldsymbol{F}$ the placement gradient and $\boldsymbol{\Delta}$ the related Green-Lagrange strain tensor:

$$\boldsymbol{F} = \nabla_X \boldsymbol{\chi} \quad \text{and} \quad \boldsymbol{\Delta} = \frac{1}{2}\left(\boldsymbol{F}\boldsymbol{F}^\top - \boldsymbol{I}\right) \tag{2}$$

where ∇_X denotes $\partial/\partial X_i$. Following the poromechanical framework [31], we introduce η, the Eulerian porosity and ϕ the Lagrangian one wich are related by $\phi = J\eta$ in which J stands for the determinant of $\boldsymbol{F}$. The solid mass conservation law in the current configuration reads as:

$$\frac{d^s}{dt}\int_{\mathcal{D}} \rho^s\,(1-\eta)\;\mathrm{d}\Omega_t = \int_{\mathcal{D}} \hat{\rho}^s\,\mathrm{d}\Omega_t \tag{3}$$

where $\hat{\rho}^s$ indicates a mass source and the intrinsic density of the solid ρ^s is constant in space and in time. According the localization theorem[33], the localized pull-back of this equation implies the following local Lagrangian form of the skeleton mass conservation law to hold true:

$$\rho^s \frac{d^s\,(J-\phi)}{dt} = \hat{\Gamma}^s \tag{4}$$

where $\hat{\Gamma}^s = J\hat{\rho}^s$ is the Lagrangian mass source.
The reference configuration of the fluid is denoted by $\mathcal{D}_0^f$ and it is related to the skeleton reference configuration via the mapping $\boldsymbol{\varrho} : \mathcal{D}_0 \times \mathcal{T} \to \mathcal{E}$. The image under $\boldsymbol{\varrho}$ of a solid particle $\boldsymbol{X}$ identifies the fluid particle $\boldsymbol{X}^f \in \mathcal{D}_0^f$ which, at time t, occupies the same current place $\boldsymbol{x}$ as that of the solid. As a consequence, the placement of the fluid phase is described by the mapping $\boldsymbol{\chi}^f$ such that $\boldsymbol{\chi}^f = \boldsymbol{\chi} \circ (\boldsymbol{\varrho})^{-1}$. We indicate with $\boldsymbol{\varrho}^{-1}$ the inverse map of $\boldsymbol{\varrho}\,(\cdot, t)$. We are now able to introduce the velocity $\boldsymbol{v}^f$ as the barycentric velocity of the 2-species fluid f. This velocity $\boldsymbol{v}^f$ is obtained by time differentiating the placement of the fluid $\boldsymbol{\chi}^f$:

$$\boldsymbol{v}^f\,(\boldsymbol{x}, t) = \frac{d\boldsymbol{\chi}^f}{dt}\left(\boldsymbol{X}^f, t\right) = \left.\frac{d\,\boldsymbol{\chi} \circ \boldsymbol{\varrho}^{-1}}{dt}\right|_{(\boldsymbol{X}^f, t)} \tag{5}$$

Applying the chain-rule, and considering $\Theta = \nabla_X \boldsymbol{\varrho}$ the fluid velocity is:

$$\boldsymbol{v}^f\,(\boldsymbol{x}, t) = \boldsymbol{v}^s\,(\boldsymbol{X}, t) - \boldsymbol{F}\,(\boldsymbol{X}, \boldsymbol{t}) \cdot \Theta\,(\boldsymbol{X}, t)^{-1} \cdot \left.\frac{\partial \boldsymbol{\varrho}}{\partial t}\right|_{(\boldsymbol{X}, t)} \tag{6}$$

Next, we denotes by $\boldsymbol{\gamma}^f$ the particle acceleration of the fluid:

$$\boldsymbol{\gamma}^f = \frac{d^f \boldsymbol{v}^f}{dt} \tag{7}$$

where d^f/dt indicates the time derivative following the motion of a fluid material particle.
Since the fluid phase is a mixture of two species, its intrinsic density ρ^f obeys the mixture theory:

$$\rho^f = \left(1 - C^f\right)\rho^{wf} + C^f \rho^s \tag{8}$$

where C^f indicates the fluidized grains volume concentration, while ρ^{wf} and ρ^s are the intrinsic densities of the pore liquid and the grains, respectively. In other words, we will assume the fluid phase to be fairly homogeneous. If considering a homogeneous binary mixture of fluidized particles and liquid is rather meaningless at the pore scale, this is otherwise admissible from the macroscopic point of view. Considering this hypothesis, we write the fluid mass balance in the current configuration:

$$\frac{d^f}{dt}\int_{\mathcal{D}} \rho^f \eta\,\mathrm{d}\Omega_t = \int_{\mathcal{D}} \hat{\rho}^f\,\mathrm{d}\Omega_t \tag{9}$$

where $\hat{\rho}^f$ is the rate of mass supplied to the fluid phase. We now introduce m^f representing the Lagrangian fluid mass content: $m^f = \phi\rho^f$ and $\boldsymbol{M}^f$ the Lagrangian filtration vector: $\boldsymbol{M}^f = \phi\rho^f \boldsymbol{F}^{-1} \cdot \left(\boldsymbol{v}^f - \boldsymbol{v}^s\right)$. Considering the Lagrangian mass source $\hat{\Gamma}^f = J\hat{\rho}^f$, we pull-back the fluid mass conservation law into the reference configuration of the solid skeleton and localise it:

$$\frac{d^s\, m^f}{dt} + \nabla_{_X} \cdot \boldsymbol{M}^f = \hat{\Gamma}^f \tag{10}$$

As usual in the framework of soil mechanics, we consider the grains incompressibility hypothesis, which links J to the Lagrangian porosity: $J - 1 = \phi - \phi_0$ where ϕ_0 is the reference (initial) Lagrangian porosity. According to Zhang et al.[30], in the case of a suffusive soil this relation is enriched introducing a new variable ϕ^{er} measuring the variation of the Lagrangian porosity induced by the sole suffusion process so that the grains incompressibility hypothesis becomes:

$$J - 1 = \phi - \phi_0 - \phi^{er} \tag{11}$$

This condition constitues a crucial point of our approach since the variation of the Langrangian porosity is no longer due just to volumetric strains but also to suffusion. Furthermore, as suffusion consists of an exchange of mass content between the solid and the fluid phases, the two mass sources $\hat{\Gamma}^s$ and $\hat{\Gamma}^f$ are opposite. For the sake of simplicity we write $\hat{\Gamma} = \hat{\Gamma}^f = -\hat{\Gamma}^s$ (leading to the Eulerian equality $\hat{\rho} = \hat{\rho}^f = -\hat{\rho}^s$). Under these assumptions, the solid and fluid mass balances become respectively:

$$\rho^s \frac{d^s\phi^{er}}{dt} = \hat{\Gamma} \quad \text{and} \quad \frac{d^s\rho^f\,(J + \phi^{er})}{dt} + \nabla_{_X} \cdot \boldsymbol{M}^f = \hat{\Gamma} \tag{12}$$

It is worth to stress that the informations about the kinetics of grains detachment and interlocking are all contained in the term $\hat{\Gamma}$ which is proportional to the time derivative of ϕ^{er} with respect to the solid motion.

3 External working

Let $\mathcal{V}^\pi(\mathcal{D})$ be the linear space of velocity fields of the phase π on $\mathcal{D}$. Let the external working $\mathcal{P}_{ext}$ be a linear continuous functional over the cartesian product $\mathcal{V}^s \times \mathcal{V}^f$ say $\mathcal{P}_{ext} : \mathcal{V}^s(\mathcal{D}) \times \mathcal{V}^f(\mathcal{D}) \to \mathbb{R}$, so that:

$$\mathcal{P}_{ext}\left(\boldsymbol{v}^s, \boldsymbol{v}^f\right) = \int_{\mathcal{D}} \boldsymbol{b}^s \cdot \boldsymbol{v}^s + \boldsymbol{b}^f \cdot \boldsymbol{v}^f \,\mathrm{d}\Omega_t + \int_{\partial\mathcal{D}} \boldsymbol{t}^s \cdot \boldsymbol{v}^s + \boldsymbol{t}^f \cdot \boldsymbol{v}^f \,\mathrm{dS}\,, \quad \left\{\boldsymbol{v}^s, \boldsymbol{v}^f\right\} \in \mathcal{V}^s \times \mathcal{V}^f \tag{13}$$

where $\boldsymbol{b}^\pi$ is the bulk force in $\mathcal{D}$ and $\boldsymbol{t}^\pi$ the surface force on the boundary $\partial\mathcal{D}$ of the current configuration. $\partial\mathcal{D}$ is required to be sufficiently regular so that it outward unit normal $\boldsymbol{n}$ can be defined almost everywhere on $\partial\mathcal{D}$. Now let $\boldsymbol{\sigma}^\pi$ be the stress acting on the phase π, such that the Cauchy stress theorem $\boldsymbol{\sigma}^\pi \cdot \boldsymbol{n} = \boldsymbol{t}^\pi$ holds true for each phase π on $\partial\mathcal{D}$. Using the Green-Ostrogradsky theorem, we obtain:

$$\int_{\partial\mathcal{D}} \boldsymbol{t}^s \cdot \boldsymbol{v}^s + \boldsymbol{t}^f \cdot \boldsymbol{v}^f \,\mathrm{dS} = \int_{\mathcal{D}} \boldsymbol{\sigma}^s : \mathbf{d}^s + (\nabla_x \cdot \boldsymbol{\sigma}^s) \cdot \boldsymbol{v}^s \,\mathrm{d}\Omega_t + \int_{\mathcal{D}} \boldsymbol{\sigma}^f : \mathbf{d}^f + \left(\nabla_x \cdot \boldsymbol{\sigma}^f\right) \cdot \boldsymbol{v}^f \,\mathrm{d}\Omega_t \tag{14}$$

Herein, the tensor $\mathbf{d}^\pi$ denotes the Eulerian strain rate tensor such that $\mathbf{d}^\pi = \left(\nabla_x \boldsymbol{v}^\pi + \nabla_x^\top \boldsymbol{v}^\pi\right)/2$ where ∇_x denotes $\partial/\partial x_i$. Replacing (14) into (13), the external working is given by the sole integral over $\mathcal{D}$:

$$\mathcal{P}_{ext}\left(\boldsymbol{v}^s, \boldsymbol{v}^f\right) = \int_{\mathcal{D}} \boldsymbol{\sigma}^s : \mathbf{d}^s + \boldsymbol{\sigma}^f : \mathbf{d}^f + (\nabla_x \cdot \boldsymbol{\sigma}^s + \boldsymbol{b}^s) \cdot \boldsymbol{v}^s + \left(\nabla_x \cdot \boldsymbol{\sigma}^f + \boldsymbol{b}^f\right) \cdot \boldsymbol{v}^f \,\mathrm{d}\Omega_t \tag{15}$$

Now focusing on the porous medium as a whole, the Cauchy stress $\boldsymbol{\sigma} = \boldsymbol{\sigma}^s + \boldsymbol{\sigma}^f$ and the overall bulk force $\boldsymbol{b} = \boldsymbol{b}^s + \boldsymbol{b}^f$ are introduced so that:

$$\mathcal{P}_{ext}\left(\boldsymbol{v}^s, \boldsymbol{v}^f\right) = \int_{\mathcal{D}} \boldsymbol{\sigma} : \mathbf{d}^s + \boldsymbol{\sigma}^f : \left(\mathbf{d}^f - \mathbf{d}^s\right) + (\nabla_x \cdot \boldsymbol{\sigma} + \boldsymbol{b}) \cdot \boldsymbol{v}^s + \left(\nabla_x \cdot \boldsymbol{\sigma}^f + \boldsymbol{b}^f\right) \cdot \left(\boldsymbol{v}^f - \boldsymbol{v}^s\right) \,\mathrm{d}\Omega_t \tag{16}$$

Recall that the balance of momentum for the overall porous medium reads as:

$$\boldsymbol{b} + \nabla_x \cdot \boldsymbol{\sigma} = \rho^s (1-\eta)\boldsymbol{\gamma}^s + \rho^f \eta \boldsymbol{\gamma}^f + \hat{\rho}\left(\boldsymbol{v}^f - \boldsymbol{v}^s\right) \tag{17}$$

while $\hat{\rho}\left(\boldsymbol{v}^f - \boldsymbol{v}^s\right)$ indicates the contribution to the time derivative of the overall momentum due to mass echange between the phases. From now on we assume that the fluid stress is linked to the fluid pressure through the Eulerian porosity, $\boldsymbol{\sigma}^f = -\eta p \boldsymbol{I}$. Hence the term $\boldsymbol{\sigma}^f : \left(\mathbf{d}^f - \mathbf{d}^s\right)$ reduces to $-\eta p \nabla_x \cdot \left(\boldsymbol{v}^f - \boldsymbol{v}^s\right)$ and $\nabla_x \cdot \boldsymbol{\sigma}^f$ to $-\nabla_x \eta p$. Finally, assuming the bulk force on the fluid to be $\boldsymbol{b}^f = \rho^f \eta \boldsymbol{f}$, equation (16) reduces to :

$$\begin{aligned} \mathcal{P}_{ext}\left(\boldsymbol{v}^s, \boldsymbol{v}^f\right) = &\int_{\mathcal{D}} \sigma : \mathbf{d}^s - \nabla_x \cdot \left(\eta p \left(\boldsymbol{v}^f - \boldsymbol{v}^s\right)\right) + \rho^f \eta \boldsymbol{f} \cdot \left(\boldsymbol{v}^f - \boldsymbol{v}^s\right) \, \mathrm{d}\Omega_t \\ &\int_{\mathcal{D}} \left(\rho^s (1-\eta)\boldsymbol{\gamma}^s + \rho^f \eta \boldsymbol{\gamma}^f\right) \cdot \boldsymbol{v}^s \, \mathrm{d}\Omega_t + \int_{\mathcal{D}} \hat{\rho} \boldsymbol{v}^s \cdot \left(\boldsymbol{v}^f - \boldsymbol{v}^s\right) \, \mathrm{d}\Omega_t \end{aligned} \tag{18}$$

In the above writing, the first integral term contains the internal working and the second the inertial effects[31]. The last integral corresponds to suffusion effects.

4 Thermodynamics

Thermodynamics of porous media is here specialized to consider the case of a suffusive soil to provide a consistent framework for the further constitutive modeling. In this section, following a similar deduction as that one proposed by Coussy[31], the two fundamental principles of thermodynamics are given in a general form in the current configuration $\mathcal{D}$. By using the above expression of the external working, a new form of the Clausius-Duhem inequality is tackled.

4.1 The first principle : internal energy

The first principle of thermodynamics states the conservation law for the internal energy of the whole porous medium. We denote by e^s and e^f the specific internal energies (i.e. per unit mass) of the solid and fluid constituents, respectively, and the specific internal energy of the porous medium (per unit volume) by $e = \rho^s (1-\eta) e^s + \rho^f \eta e^f$. The first principle, written in the current configuration reads as:

$$\mathcal{P}_{ext} + \mathring{\mathcal{Q}} = \frac{d^s}{dt} \int_{\mathcal{D}} \rho^s (1-\eta) \left(e^s + \frac{\boldsymbol{v}^s \cdot \boldsymbol{v}^s}{2}\right) \, \mathrm{d}\Omega_t + \frac{d^f}{dt} \int_{\mathcal{D}} \rho^f \eta \left(e^f + \frac{\boldsymbol{v}^f \cdot \boldsymbol{v}^f}{2}\right) \, \mathrm{d}\Omega_t \tag{19}$$

where $\mathcal{P}_{ext}$ is the external working and $\mathring{\mathcal{Q}}$ the heat source represented in terms of a heat flux through the boundary $\partial\mathcal{D}$:

$$\mathring{\mathcal{Q}} = \int_{\partial\mathcal{D}} -\boldsymbol{q} \cdot \boldsymbol{n} \, \mathrm{dS} = \int_{\mathcal{D}} -\nabla_x \cdot \boldsymbol{q} \, \mathrm{d}\Omega_t \tag{20}$$

To highlight the effect of mass transfer (suffusion), the time derivative of the kinetic energy of each phase is rewritten making use of the mass conservation laws. Thus time derivative of the solid kinetic energy is given by:

$$\begin{aligned} \frac{d^s}{dt} \int_{\mathcal{D}} \rho^s (1-\eta) \frac{\boldsymbol{v}^s \cdot \boldsymbol{v}^s}{2} \, \mathrm{d}\Omega_t = &\frac{1}{2} \int_{\mathcal{D}} \left(\frac{\partial \rho^s (1-\eta)}{\partial t} + \nabla_x \cdot \left(\rho^s (1-\eta) \boldsymbol{v}^s\right)\right) \boldsymbol{v}^s \cdot \boldsymbol{v}^s \, \mathrm{d}\Omega_t \\ &+ \frac{1}{2} \int_{\mathcal{D}} \left(\frac{\partial \boldsymbol{v}^s \cdot \boldsymbol{v}^s}{\partial t} + \nabla_x \cdot \left(\left(\boldsymbol{v}^s \cdot \boldsymbol{v}^s\right) \boldsymbol{v}^s\right)\right) \rho^s (1-\eta) \, \mathrm{d}\Omega_t \end{aligned} \tag{21}$$

reformulated in the following form:

$$\frac{d^s}{dt} \int_{\mathcal{D}} \rho^s (1-\eta) \frac{\boldsymbol{v}^s \cdot \boldsymbol{v}^s}{2} \, \mathrm{d}\Omega_t = \int_{\mathcal{D}} -\frac{1}{2} \hat{\rho} \boldsymbol{v}^s \cdot \boldsymbol{v}^s + \rho^s (1-\eta) \boldsymbol{\gamma}^s \cdot \boldsymbol{v}^s, \mathrm{d}\Omega_t \tag{22}$$

Similary the time derivative of the fluid kinetic energy is given by:

$$\frac{d^f}{dt}\int_{\mathcal{D}} \rho^f \eta \frac{\boldsymbol{v}^f \cdot \boldsymbol{v}^f}{2}\,\mathrm{d}\Omega_t = \int_{\mathcal{D}} \frac{1}{2}\hat{\rho}\boldsymbol{v}^f \cdot \boldsymbol{v}^f + \rho^f \eta \boldsymbol{\gamma}^f \cdot \boldsymbol{v}^f, \mathrm{d}\Omega_t \tag{23}$$

Equations (22) and (23) show that the term $\hat{\rho}$ is explicitly taken into account in the time derivative of the kinetic energies. Moreover, as usual in poromechanics[31], the time derivatives of the internal energies of the solid and the fluid can be rearranged as follows:

$$\frac{d^s}{dt}\int_{\mathcal{D}} \rho^s (1-\eta) e^s \,\mathrm{d}\Omega_t + \frac{d^f}{dt}\int_{\mathcal{D}} \rho^f \eta e^f \,\mathrm{d}\Omega_t = \int_{\mathcal{D}} \frac{d^s e}{dt} + e\nabla_x \cdot \boldsymbol{v}^s + \nabla_x \cdot \left(\rho^f \eta e^f \left(\boldsymbol{v}^f - \boldsymbol{v}^s\right)\right) \mathrm{d}\Omega_t \tag{24}$$

Replacing equations (18), (22), (23) and (24) in (19) and introducing the specific enthalpy of the fluid $h^f = e^f + \dfrac{p}{\rho^f}$, we get the global Eulerian formulation of the first principle of thermodynamics for a suffusive porous medium:

$$\int_{\mathcal{D}} \boldsymbol{\sigma} : \mathbf{d}^s - \nabla_x \cdot \left(\rho^f \eta h^f \left(\boldsymbol{v}^f - \boldsymbol{v}^s\right)\right) + \left(\rho^f \eta \left(\boldsymbol{f} - \boldsymbol{\gamma}^f\right) - \frac{1}{2}\hat{\rho}\left(\boldsymbol{v}^f - \boldsymbol{v}^s\right)\right) \cdot \left(\boldsymbol{v}^f - \boldsymbol{v}^s\right) - \nabla_x \cdot \boldsymbol{q}\,\mathrm{d}\Omega_t = \frac{d^s}{dt}\int_{\mathcal{D}} e\,\mathrm{d}\Omega_t \tag{25}$$

With the aim of providing the local Lagrangian form of the first principle of thermodynamics, we introduce the Lagrangian quantities: $E = eJ$ the total Lagrangian internal energy of the porous medium, $\Sigma = J\boldsymbol{F}^{-1} \cdot \boldsymbol{\sigma} \cdot \boldsymbol{F}^{-\top}$ the second Piola-Kirchhoff overall stress tensor, and $\boldsymbol{Q} = J\boldsymbol{q}$ the pull back of the Eulerian heat-flux in the reference configuration. We localise the pull-back of (25) in $\mathcal{D}_0$. In this way, the local Lagrangian form of the first principle is provided by:

$$\frac{d^s E}{dt} = \boldsymbol{\Sigma} : \frac{d^s \boldsymbol{\Delta}}{dt} - \nabla_X \cdot \left(h^f \boldsymbol{M}^f\right) + \left(\boldsymbol{f} - \boldsymbol{\gamma}^f - \frac{\hat{\Gamma}}{2\left(\rho^f \phi\right)^2}\boldsymbol{F} \cdot \boldsymbol{M}^f\right) \cdot \left(\boldsymbol{F} \cdot \boldsymbol{M}^f\right) - \nabla_X \cdot \boldsymbol{Q} \tag{26}$$

4.2 The second principle : entropy

The second principle of thermodynamics expresses the balance of entropy. We denote by s^s and s^f the specific entropies (i.e. per unit mass) of the solid and fluid phases, respectively. Then the specific entropy of the porous medium (per unit volume) is given by $s = \rho^s (1-\eta) s^s + \rho^f \eta s^f$. The entropy balance, written on the current configuration, is:

$$\frac{d^s}{dt}\int_{\mathcal{D}} \rho^s (1-\eta) s^s \,\mathrm{d}\Omega_t + \frac{d^f}{dt}\int_{\mathcal{D}} \rho^f \eta s^f \,\mathrm{d}\Omega_t \geqslant \int_{\partial\mathcal{D}} -\frac{\boldsymbol{q}\cdot\boldsymbol{n}}{T}\,\mathrm{dS} \tag{27}$$

where T is the overall absolute temperature. Developing a similar procedure as the one considered for the first principle, the second principle is pull-back into the reference configuration $\mathcal{D}_0$ and the local Lagrangian form reads:

$$\frac{d^s S}{dt} \geqslant -\nabla_X \cdot \left(s^f \boldsymbol{M}^f + \frac{\boldsymbol{Q}}{T}\right) \tag{28}$$

S being the Lagrangian entropy of the porous medium as a whole.

4.3 The Clausius-Duhem inequality

From now on and for the sake of simplicity, for any quantity a, $\dot{a}$ denotes its time derivative with respect to the motion of the skeleton (i.e. $d^s a/dt$). The Clausius-Duhem inequality is now tackled with the aim of

identifying the thermodynamical dissipation of a suffusive soil. This will allow for stating suitable restrictions on the constitutive laws.
We introduce the Helmoltz free energy of the porous medium $\Psi = E - TS$, so that the second principle can be re-written as:

$$\dot{S} = \frac{1}{T}\left(\dot{E} - S\dot{T} - \dot{\Psi}\right) \geqslant -\nabla_X \cdot \left(s^f \boldsymbol{M}^f + \frac{\boldsymbol{Q}}{T}\right) \tag{29}$$

Let Ψ^s be the Helmoltz free energy of the solid and ψ^f the specific Helmoltz free energy of the fluid such that $\Psi = \Psi^s + m^f \psi^f$. Using the first principle (26) in (29) multiplied by T, we finally get the thermodynamical dissipation Φ that is to say the Clausius-Duhem inequality :

$$\begin{aligned}\Phi = &\left(\boldsymbol{\Sigma} : \dot{\boldsymbol{\Delta}} - \nabla_X \cdot \left(h^f \boldsymbol{M}^f\right) + \left(\boldsymbol{f} - \boldsymbol{\gamma}^f - \frac{\hat{\Gamma}}{2\left(\rho^f \phi\right)^2}\boldsymbol{F} \cdot \boldsymbol{M}^f\right) \cdot \left(\boldsymbol{F} \cdot \boldsymbol{M}^f\right) - \nabla_X \cdot \boldsymbol{Q}\right) \\ &- S\dot{T} - \dot{\Psi}^s - \left(\dot{m}^f \psi^f + m^f \dot{\psi}^f\right) + \nabla_X \cdot \left(s^f \boldsymbol{M}^f + \frac{\boldsymbol{Q}}{T}\right) T \geqslant 0\end{aligned} \tag{30}$$

In order to provide the framework within which constitutive prescriptions for the solid skeleton can be stated, cumbersome calculations are needed. The main steps are : (i) to consider the constitutive law of the fluid phase as simple as possible:

$$p = -\frac{\partial \psi^f}{\partial (1/\rho^f)} \qquad \text{and} \qquad s^f = -\frac{\partial \psi^f}{\partial T} \tag{31}$$

(ii) to use the definition of the Gibbs potential of the fluid as $g^f = \psi^f + p/\rho^f$ and $g^f = h^f + Ts^f$, and (iii) to consider the solid free energy as a function of T, $\boldsymbol{\Delta}$ and $\boldsymbol{\zeta}$: $\Psi^s = \Psi^s\left(T, \boldsymbol{\Delta}, \boldsymbol{\zeta}\right)$ where $\boldsymbol{\zeta}$ is a generalized internal variable vector accounting for irreversible processes occuring within the solid skeleton. Each component α of $\boldsymbol{\zeta}$ (i.e. ζ_α) may present a different order of tensoriality. In particular, among others, $\boldsymbol{\zeta}$ will include the scalar quantity ϕ^{er}. The Clausius-Duhem inequality is now splitted in three terms. The two first terms of $\Phi^s_{\rightarrow}$ essentially describes the dissipation due to irreversible deformations and mechanical effects of suffusion, $\Phi^f_{\rightarrow}$ gathers both the hydraulic diffusion and the suffusion evolution; finally the last contribution Φ^t, is the dissipation linked to thermal effects. Due to its classical form, we suggest as usual that Φ^t is positive but we don't state for any positivity restricions over $\Phi^s_{\rightarrow}$ and $\Phi^f_{\rightarrow}$ right-now due to their unusual forms. Consequently, we write the Clausius-Duhem inequality as $\Phi = \Phi^s_{\rightarrow} + \Phi^f_{\rightarrow} + \Phi^t \geqslant 0$.

$$\Phi^s_{\rightarrow} = \left(\boldsymbol{\Sigma} + pJ\boldsymbol{F}^{-1} \cdot \boldsymbol{F}^{-\top} - \frac{\partial \Psi^s}{\partial \boldsymbol{\Delta}}\right) : \dot{\boldsymbol{\Delta}} - \left\langle \frac{\partial \Psi^s}{\partial \zeta_\alpha}, \dot{\zeta}_\alpha \right\rangle - \left(S^s + \frac{\partial \Psi^s}{\partial T}\right)\dot{T} \tag{32a}$$

$$\Phi^f_{\rightarrow} = \left(-\frac{1}{\rho^f}\nabla_x p + \left(\boldsymbol{f} - \boldsymbol{\gamma}^f\right)^\top \cdot \boldsymbol{F}\right) \cdot \boldsymbol{M}^f + \left(p\left(1 - \frac{\rho^s}{\rho^f}\right) - \frac{\rho^s}{2\left(\rho^f \phi\right)^2}\left(\boldsymbol{F} \cdot \boldsymbol{M}^f\right)^2\right)\dot{\phi}^{er} \tag{32b}$$

$$\Phi^t = -\frac{\boldsymbol{Q}}{T} \cdot \nabla_x T \geqslant 0 \tag{32c}$$

where $\langle \partial \Psi^s / \partial \zeta_\alpha, \dot{\zeta}_\alpha \rangle$ denotes the inner product over the space to which belongs the α-th component of $\boldsymbol{\zeta}$. The index $\rightarrow$ indicates the presence of suffusion effects on both $\Phi^s_{\rightarrow}$ and $\Phi^f_{\rightarrow}$. One of the aims of the next section is to identify more clearly the whole effect of suffusion and rephrase the Clausius-Duhem inequality as $\Phi = \Phi^s + \Phi^f + \Phi^t \geqslant 0$. In this targeted form, we identify three uncoupled dissipation sources: the first, Φ^s, is related to the skeleton behaviour, the second, Φ^f, is linked the hydraulic diffusion and every explicit suffusion's effects, the thermal dissipation, Φ^t, remaining unchanged. Each dissipation is supposed to be positive. From such a formulation, we will deduce the constitutive restrictions related to mechanical behaviour, hydraulic diffusion, suffusion kinetics and thermal diffusion.

5 Constitutive modelling

In this section, we explore the possible constitutive modelling of a suffusive soil, focusing especially on the coupling between the suffusion and both seepage flow and the mechanical state of the skeleton.

5.1 Constitutive prescriptions for the skeleton behaviour

The dissipation term of equation (32a) is similar to the one used to describe the effects of dissolution (see Coussy[31]). If for the sake of simplicity, isothermal conditions so $\dot{T} = 0$ are assumed, the dependency of Ψ^s on the temperature can be omitted and the first term of the dissipation reduces to:

$$\Phi^s_{\rightarrow} = \left(\boldsymbol{\Sigma} + pJ\boldsymbol{F}^{-1} \cdot \boldsymbol{F}^{-\top} - \frac{\partial \Psi^s}{\partial \boldsymbol{\Delta}} \right) : \dot{\boldsymbol{\Delta}} - \left\langle \frac{\partial \Psi^s}{\partial \boldsymbol{\zeta}}, \dot{\boldsymbol{\zeta}} \right\rangle \tag{33}$$

From now on the small strains hypothesis is taken into account, so that the Green-Lagrange strain tensor $\boldsymbol{\Delta}$ is equal to the linearised strain tensor $\boldsymbol{\varepsilon}$. Moreover, we assume the reference configuration to be stress free, which allows to identify the value of the Cauchy stress tensor $\boldsymbol{\sigma}$ with that of the second Piola-Kirchhoff stress tensor $\boldsymbol{\Sigma}$. As a consequence, the Terzaghi effective stress tensor $\boldsymbol{\sigma}' = \boldsymbol{\sigma} + p$ can be introduced:

$$\Phi^s_{\rightarrow} = \left(\boldsymbol{\sigma}' - \frac{\partial \Psi^s}{\partial \boldsymbol{\varepsilon}} \right) : \dot{\boldsymbol{\varepsilon}} - \left\langle \frac{\partial \Psi^s}{\partial \boldsymbol{\zeta}}, \dot{\boldsymbol{\zeta}} \right\rangle \tag{34}$$

the hypothesis of small strains moreover yields: $\boldsymbol{\varepsilon} = \boldsymbol{\varepsilon}^e + \boldsymbol{\varepsilon}^p$, where $\boldsymbol{\varepsilon}^e$ and $\boldsymbol{\varepsilon}^p$ are the elastic and plastic strain tensors, respectively. Grain incompressibility stated in equation (11) is therefore rephrased by partitionning the porosity ϕ into a reversible contribution ϕ^e and an irreversible one denoted ϕ^p:

$$\varepsilon^e_v + \varepsilon^p_v = \phi^e + \phi^p - \phi^{er} - \phi_0 \tag{35}$$

where ε^e_v and ε^p_v are, respectively, the elastic and plastic volumetric strains. In particular, the irreversible contributions into equation (35) are required to verify:

$$\phi^p = \phi^{er} + \varepsilon^p_v \tag{36}$$

Next, we identify the internal variables as the current value of the plastic strain tensor $\boldsymbol{\varepsilon}^p$ and the suffusion induced porosity ϕ^{er} as well as that of the cumulated plastic strain $\bar{\epsilon}^p$:

$$\bar{\epsilon}^p(t) = \int_0^t \sqrt{\dot{\boldsymbol{\varepsilon}}^p_d(\tau) : \dot{\boldsymbol{\varepsilon}}^p_d(\tau)} \mathrm{d}\tau \tag{37}$$

$\boldsymbol{\varepsilon}_d$ being the deviatoric strain tensor. Thus with slight abuse of notation, the solid free energy is represented by: $\Psi^s = \Psi^s(\boldsymbol{\varepsilon}, \boldsymbol{\varepsilon}^p, \bar{\epsilon}^p, \phi^{er})$. More specifically, we suggest to split Ψ^s in two contributions with respect to the skeleton behaviour: an elastic one which depends on the elastic strain tensor and the suffusion induced porosity: $\Psi^s_e(\boldsymbol{\varepsilon} - \boldsymbol{\varepsilon}^p, \phi^{er})$ and the frozen or plastic one which depends only on the internal variables: $\Psi^s_p(\boldsymbol{\varepsilon}^p, \bar{\epsilon}^p, \phi^{er})$. According to these assumptions, we assume that the suffusion induced porosity affects both the elastic and the frozen free energies: the dependency of Ψ^s_e on ϕ^{er} accounts for the effects of erosion as a kind of damage parameter which modifies the stiffness of the solid skeleton; the dependency of Ψ^s_p on ϕ^{er} conversely is similar to the one of a softening or hardening variable.
Thus assuming the following expression of the solid free energy: $\Psi^s = \Psi^s_e(\boldsymbol{\varepsilon} - \boldsymbol{\varepsilon}^p, \phi^{er}) + \Psi^s_p(\boldsymbol{\varepsilon}^p, \bar{\epsilon}^p, \phi^{er})$ we write the skeleton dissipation as follows:

$$\Phi^s_{\rightarrow} = \left(\boldsymbol{\sigma}' - \frac{\partial \Psi^s_e}{\partial(\boldsymbol{\varepsilon} - \boldsymbol{\varepsilon}^p)} \right) : (\dot{\boldsymbol{\varepsilon}} - \dot{\boldsymbol{\varepsilon}}^p) + \boldsymbol{\sigma}' : \dot{\boldsymbol{\varepsilon}}^p - \frac{\partial \Psi^s_p}{\partial \boldsymbol{\varepsilon}^p} : \dot{\boldsymbol{\varepsilon}}^p - \frac{\partial \Psi^s_p}{\partial \bar{\epsilon}^p} \dot{\bar{\epsilon}}^p - \left(\frac{\partial \Psi^s_e}{\partial \phi^{er}} + \frac{\partial \Psi^s_p}{\partial \phi^{er}} \right) \dot{\phi}^{er} \tag{38}$$

Separating the plastic strain into its spherical and deviatoric components one has:

$$\Phi^s_{\rightarrow} = \left(\boldsymbol{\sigma}' - \frac{\partial \Psi^s_e}{\partial\left(\boldsymbol{\varepsilon} - \boldsymbol{\varepsilon}^p\right)}\right) : \left(\dot{\boldsymbol{\varepsilon}} - \dot{\boldsymbol{\varepsilon}}^p\right) + \boldsymbol{\sigma}' : \dot{\boldsymbol{\varepsilon}}^p - \frac{\partial \Psi^s_p}{\partial \boldsymbol{\varepsilon}^p_d} : \dot{\boldsymbol{\varepsilon}}^p_d - \frac{\partial \Psi^s_p}{\partial \varepsilon^p_v}\dot{\varepsilon}^p_v - \frac{\partial \Psi^s_p}{\partial \bar{\epsilon}^p}\dot{\bar{\epsilon}}^p - \left(\frac{\partial \Psi^s_e}{\partial \phi^{er}} + \frac{\partial \Psi^s_p}{\partial \phi^{er}}\right)\dot{\phi}^{er} \tag{39}$$

If equation (36) is used within the frozen free energy, the following change of variable $\Psi^s_p\left(\boldsymbol{\varepsilon}^p_d, \varepsilon^p_v, \bar{\epsilon}^p, \phi^{er}\right) = \Psi^s_p\left(\boldsymbol{\varepsilon}^p_d, \phi^p, \bar{\epsilon}^p\right)$ can be made, so that Ψ^s_p depends on $\boldsymbol{\varepsilon}^p_v$ and ϕ^{er} via ϕ^p:

$$\frac{\partial \Psi^s_p}{\partial \varepsilon^p_v}\dot{\varepsilon}^p_v + \frac{\partial \Psi^s_p}{\partial \phi^{er}}\dot{\phi}^{er} = \frac{\partial \Psi^s_p}{\partial \phi^p}\dot{\phi}^p \tag{40}$$

As a consequence, the term $\left(\partial \Psi^s_e / \partial \phi^{er}\right)\dot{\phi}^{er}$ is the sole term explicitely linked to the suffusion kinetics, which in fact motivates the choice to make it part of the fluid dissipation Φ^f rather than the solid one.
Accordingly the skeleton dissipation Φ^s is required to be positive definite and writes:

$$\begin{aligned}\Phi^s &= \Phi^s_{\rightarrow} + \frac{\partial \Psi^s_e}{\phi^{er}}\dot{\phi}^{er} \geqslant 0 \\ &= \left(\boldsymbol{\sigma}' - \frac{\partial \Psi^s_e}{\partial\left(\boldsymbol{\varepsilon} - \boldsymbol{\varepsilon}^p\right)}\right) : \left(\dot{\boldsymbol{\varepsilon}} - \dot{\boldsymbol{\varepsilon}}^p\right) + \boldsymbol{\sigma}' : \dot{\boldsymbol{\varepsilon}}^p - \frac{\partial \Psi^s_p}{\partial \boldsymbol{\varepsilon}^p_d} : \dot{\boldsymbol{\varepsilon}}^p_d - \frac{\partial \Psi^s_p}{\partial \phi^p}\dot{\phi}^p - \frac{\partial \Psi^s_p}{\partial \bar{\epsilon}^p}\dot{\bar{\epsilon}}^p \geqslant 0\end{aligned} \tag{41}$$

Similarly, the fluid dissipation Φ^f, including from now-on the suffusion effects, is rephrased and assumed to be positive definite:

$$\begin{aligned}\Phi^f &= \Phi^f_{\rightarrow} - \frac{\partial \Psi^s_e}{\phi^{er}}\dot{\phi}^{er} \geqslant 0 \\ &= \left(-\frac{1}{\rho^f}\nabla_x p + \left(\boldsymbol{f} - \boldsymbol{\gamma}^f\right)\right) \cdot \boldsymbol{M}^f + \left(p\left(1 - \frac{\rho^s}{\rho^f}\right) - \frac{\partial \Psi^s_e}{\partial \phi^{er}}\right)\dot{\phi}^{er} \geqslant 0\end{aligned} \tag{42}$$

Here, we have also assumed the fluid velocity to be small enough so that the contribution of the squared filtration vector can be neglected. For purely elastic transformations, no dissipation occurs ($\Phi^s = 0$) and the internal variable set remains constant, then the elastic constitutive law is given by:

$$\boldsymbol{\sigma}' = \frac{\partial \Psi^s_e}{\partial\left(\boldsymbol{\varepsilon} - \boldsymbol{\varepsilon}^p\right)} \tag{43}$$

Let Ψ^s_e be a quadratic form such that $\Psi^s_e = \left(\boldsymbol{\varepsilon} - \boldsymbol{\varepsilon}^p\right) : \mathbb{C}\left(\phi^{er}\right) : \left(\boldsymbol{\varepsilon} - \boldsymbol{\varepsilon}^p\right)/2 + \Psi^s_{e0}$, where $\mathbb{C}$ is the classical elastic stiffness tensor and Ψ^s_{e0} a reference free energy. The stress-strain relation becomes:

$$\boldsymbol{\sigma}' = \mathbb{C}\left(\phi^{er}\right) : \left(\boldsymbol{\varepsilon} - \boldsymbol{\varepsilon}^p\right) \tag{44}$$

We notice that $\mathbb{C}$ possibily depends on ϕ^{er} as a kind of damage parameter see for e.g. Zhang et al.[30], the purely dissipative part of Φ^s is therefore:

$$\Phi^s = \boldsymbol{\sigma}' : \dot{\boldsymbol{\varepsilon}}^p - \frac{\partial \Psi^s_p}{\partial \boldsymbol{\varepsilon}^p_d} : \dot{\boldsymbol{\varepsilon}}^p_d - \frac{\partial \Psi^s_p}{\partial \phi^p}\dot{\phi}^p - \frac{\partial \Psi^s_p}{\partial \bar{\epsilon}^p}\dot{\bar{\epsilon}}^p \geqslant 0 \tag{45}$$

where we identify $\partial \Psi^s_p / \partial \boldsymbol{\varepsilon}^p_d$ as a kinematic hardening force, $\partial \Psi^s_p / \partial \phi^p$ and $\partial \Psi^s_p / \partial \bar{\epsilon}^p$ as isotropic hardening forces. In order to ensure the positivity of such a formal dissipation, we shall formulate a constitutive model in the framework of elasto-plasticity parametrized by the irreversible porosity variation $\dot{\phi}^p$ (Section 6).

5.2 Hydromechanics: coupling fluid diffusion and suffusion

We now focus on the fluid dissipation (42). Basically, the first term is the classical Darcy contribution: considering a non-suffusive process say assuming $\dot{\phi}^{er} = 0$ leads to the following fluid dissipation:

$$\left(-\frac{1}{\rho^f}\nabla_x p + \left(\boldsymbol{f} - \boldsymbol{\gamma}^f\right)\right) \cdot \boldsymbol{M}^f \geqslant 0 \tag{46}$$

which obviously implies the Darcy law to hold true.

$$\boldsymbol{M}^f = \mathcal{K} \cdot \left(-\frac{1}{\rho^f} \nabla_x p + \left(\boldsymbol{f} - \boldsymbol{\gamma}^f \right) \right) \tag{47}$$

where $\mathcal{K}$ is the symmetrical, positive definite permeability tensor. The second term of the inequality (42) is related to suffusion $\dot{\phi}^{er}$. Let us consider a purely suffusive process (i.e. $\boldsymbol{M}^f = \boldsymbol{0}$), the fluid dissipation reduces to:

$$\left(p \left(1 - \frac{\rho^s}{\rho^f} \right) - \frac{\partial \Psi_e^s}{\partial \phi^{er}} \right) \dot{\phi}^{er} \geqslant 0 \tag{48}$$

To ensure the positivity of the dissipation, we can therefore state a linear relationship such that:

$$\dot{\phi}^{er} = \mathcal{R} \left(p \left(1 - \frac{\rho^s}{\rho^f} \right) - \frac{\partial \Psi_e^s}{\partial \phi^{er}} \right) \geqslant 0 \tag{49}$$

$\mathcal{R}$ being a positive suffusional admittance: the larger $\mathcal{R}$, the larger $\dot{\phi}^{er}$. The stationary condition is reached when the suffusive dissipation vanishes and reads as:

$$\frac{\partial \Psi_e^s}{\partial \phi^{er}} = p \left(1 - \frac{\rho^s}{\rho^f} \right) \tag{50}$$

However, it is experimentally observed[4, 5, 6, 7, 8, 9, 10, 11, 12, 13, 15] that the suffusion rate is highly dependent on seepage forces. Indeed, equation (42) suggests to introduce a linear symmetric coupling between the fluxes $\boldsymbol{M}^f$ and $\dot{\phi}^{er}$ and the corresponding thermodynamic forces to enforce the positivity of Φ^f via the positive definiteness of the coupling tensor. In this way, we extend the rationale leading to equations (47) and (49) to the case when flow and suffusion are strongly coupled. As previously done for the uncoupled analysis, a linear relationship is assumed between fluxes and forces, in the spirit of extended thermodynamics:

$$\begin{pmatrix} \boldsymbol{M}^f \\ \dot{\phi}^{er} \end{pmatrix} = \begin{Bmatrix} \mathcal{K} & \mathcal{C} \\ \mathcal{C} & \mathcal{R} \end{Bmatrix} \cdot \begin{pmatrix} -\frac{1}{\rho^f} \nabla_x p + \left(\boldsymbol{f} - \boldsymbol{\gamma}^f \right) \\ p \left(1 - \frac{\rho^s}{\rho^f} \right) - \frac{\partial \Psi_e^s}{\partial \phi^{er}} \end{pmatrix} \tag{51}$$

where $\mathcal{C}$ indicates a coupling vector which should guarantee the determinant of the coupling tensor to be positive. The meaning of $\mathcal{C}$ is a crucial point of this development. Equation (51) implies on the one hand that the porosity variation due to suffusion $\left(\dot{\phi}^{er} \right)$ is driven by the gradient of fluid pressure, corroborating previous research results[23, 24, 25, 26, 27, 28]; on other hand, the proposed law implies an effect of suffusion on the seepage flow. In other words, the filtration vector is not only prescribed by the pressure gradient as in the classical Darcy law but it can also be affected by suffusion effects. At this stage, we provide only a constitutive prescription and no assumption on the magnitude of the fluxes (direct or coupled) is made. Equation (51) seems to be a relevant starting point for future works, devoted to the identification of the constitutive parameters. Laboratory scale experimental activities as well as multi-scale numerical modelling could be developed.

5.3 Thermal diffusion

Regarding the thermal dissipation, the positivity is ensured using the Fourrier law $\boldsymbol{Q} = -\boldsymbol{\kappa}_{th} \cdot \nabla_X T$, where $\boldsymbol{\kappa}_{th}$ is the thermal conductivity tensor, diagonal and positive definite.

6 A porosity-dependent plasticity model for suffusive soils

With the aim of proposing an elasto-plasticity model accounting for changes in porosity due to suffusion, we extend the Nova "Sinfonietta-Classica" model which combines the advantages of the Cam-Clay model and the Mastuoka-Nakai failure criterion[32]. This is a non-associated model which considers the preconsolidation pressure p_c as an isotropic hardening variable, depending on the whole plastic strain tensor $\boldsymbol{\varepsilon}^p$. Similar to the Cam-Clay model, Sinfonietta-Classica is a cap model, which means that it restricts pure compressive stress states to finite values: if p_c is the preconsolidation pressure, then for cohesionless soils, $p' \in]0, p_c]$, p' being the mean effective pressure. However, unlike the Cam-Clay model, Sinfonietta-Classica well captures the behaviour of sands and soft-rocks, especially during monotonic loadings. The original Sinfonietta-Classica model was not designed to handle porous media characterised by a degradable solid matrix. The adopted approach can be extended to other models stated in the same spirit as the Cam-Clay model.

6.1 Flow rule, plastic potential and loading surface

We denote by $\mathbb{T}_s^2$ the space of symmetric second-order tensors. As usual in the theory of plasticity[34], we assume the existence of a yielding function f defined over the cartesian product $\mathbb{T}_s^2 \times \mathbb{R}$ taking values in $\mathbb{R}$

$$\begin{array}{rccc} f & : & \mathbb{T}_s^2 \times \mathbb{R} & \rightarrow & \mathbb{R} \\ & & (\boldsymbol{\sigma}', p_c) & \mapsto & f(\boldsymbol{\sigma}', p_c) \end{array} \tag{52}$$

$\boldsymbol{\sigma}'$ being the effective stress and p_c a hardening force which in this case is represented by the preconsolidation pressure. The subdomain of $\mathbb{T}_s^2 \times \mathbb{R}$ where f is negative is called the elastic domain $\mathbb{S}$. The part of $\mathbb{T}_s^2$ on which the value of f is 0 is defined as the loading surface $\partial\mathbb{S}$.

$$\mathbb{S} := \left\{(\boldsymbol{\sigma}', p_c) \in \mathbb{T}_s^2 \times \mathbb{R} \,|\, f(\boldsymbol{\sigma}', p_c) < 0\right\} \quad ; \quad \partial\mathbb{S} := \left\{(\boldsymbol{\sigma}', p_c) \in \mathbb{T}_s^2 \times \mathbb{R} \,|\, f(\boldsymbol{\sigma}', p_c) = 0\right\} \tag{53}$$

The union of $\mathbb{S}$ and $\partial\mathbb{S}$ (which is nothing else than the closure $\overline{\mathbb{S}}$ of $\mathbb{S}$) defines the subdomain of plastically admissible states. Evolutions of the plastic strain tensor occurs for a mechanical state implying $f(\boldsymbol{\sigma}', p_c) = 0$ and $\dot{f}(\boldsymbol{\sigma}', p_c) = 0$. If one of this two conditions is not fulfilled, the strain evolution remains purely elastic. For non-associated plasticity, which is the case of the Sinfonietta-Classica model, the evolution of the plastic strain tensor is assigned by means of a plastic potential g:

$$\dot{\boldsymbol{\varepsilon}}^p = \dot{\lambda} \frac{\partial g}{\partial \boldsymbol{\sigma}'} \tag{54}$$

where $\dot{\lambda} \geqslant 0$ is the so-called plastic multiplier. A hardening/softening law is normally postulated for the hardening force as a function of suitable hardening variables. For Cam-Clay based models, this hardening law relates the evolution of the preconsolidation pressure p_c to the increment of the volumetric plastic strain and, eventually, to the increment of the deviatoric plastic strain tensor. Due to grain incompressibility, the increment of the volumetric plastic strain indeed is representative of the increment of the irreversible porosity $\dot{\phi}^p$

Let p' be the mean effective pressure such that $p' = -1/3 Tr(\boldsymbol{\sigma}')$ and $\boldsymbol{s}'$ the deviatoric part of $\boldsymbol{\sigma}'$, the second invariant of $\boldsymbol{s}'$ is denoted $J_2 = \boldsymbol{s}' : \boldsymbol{s}'/2$; moreover we define the deviatoric stress q as $q = \sqrt{3J_2}$. We then introduce the stress ratio tensor $\boldsymbol{\xi} = \boldsymbol{s}'/p'$ and the stress ratio $\xi = q/p'$. The second and third invariants of $\boldsymbol{\xi}$ are denoted by $J_{2\boldsymbol{\xi}}$ and $J_{3\boldsymbol{\xi}}$ such that $J_{2\boldsymbol{\xi}} = \boldsymbol{\xi} : \boldsymbol{\xi}$ and $J_{3\boldsymbol{\xi}} = 3\det(\boldsymbol{\xi})$. As for the original Sinfonietta-Classica plastic model, the yielding function f and the plastic potential g are:

$$f(\boldsymbol{\sigma}', p_c) = 3\beta(\mu - 3) \ln \frac{p'}{p_c} + \frac{9}{4}(\mu - 1) J_{2\boldsymbol{\xi}} + \mu J_{3\boldsymbol{\xi}} \leqslant 0 \tag{55a}$$

$$g\left(\boldsymbol{\sigma}', p_g\right) = 9\left(\mu - 3\right)\ln\frac{p'}{p_g} + \frac{9}{4}\left(\mu - 1\right)J_{2\boldsymbol{\xi}} + \mu J_{3\boldsymbol{\xi}} \tag{55b}$$

where β is a non-dimensionnal quantity characterizing the deviation from associativity: if $\beta = 3$, then the plastic behaviour of the soil is associated and normality rule holds true. The second non-dimensionnal parameter μ is defined by $\mu = \left(9 - Z^2\right)/\left(3 - Z^2 + 2Z^3/9\right)$ where Z denotes the slope of the characteristic state line: $Z = 6\sin\varphi/\left(3 - \sin\varphi\right)$, function of the friction angle φ measured at the zero-dilatance point in drained axisymmetric triaxial test. This line describe the transition from contractive to dilative behaviour of the soil. From the two sides of the characteristic state line, the volumetric plastic behaviour of the soil is different: if the stress state is such that $\xi > Z$ then the soil behaviour is dilative, inversely if $\xi < Z$ the soil is contractive. The limit case being $\xi = Z$, in this case, the soil is plastically incompressible. The parameter p_g should be non-zero and positive but the knwoledge of its value is of no importance since only the derivative of g with respect to $\boldsymbol{\sigma}'$ is considered in all computations.
Dilatancy is defined as the ratio between the volumetric plastic strain and the norm of the deviatoric plastic strain. According to the flow rule, it is given by:

$$d = -\frac{\dot{\varepsilon}_v^p}{\|\dot{\boldsymbol{\varepsilon}}_d^p\|} = -\frac{\dfrac{\partial g}{\partial \boldsymbol{\sigma}'} : \boldsymbol{I}}{\left\|\mathbb{P} : \dfrac{\partial g}{\partial \boldsymbol{\sigma}'}\right\|} \tag{56}$$

where $\mathbb{P}$ stands for the deviatoric projection tensor such that $\mathbb{P} = \mathbb{I} - \boldsymbol{I}\otimes\boldsymbol{I}/3$, $\mathbb{I}$ being the fourth order identity tensor and $\otimes$ the tensorial product. In axisymmetric conditions, we reduce $J_{2\xi}$ to $2\xi^2/3$ and $J_{3\xi}$ to $2\xi^3/9$. Then, the dilatancy reads:

$$d = -\frac{\dfrac{2}{9}\mu\xi^3 - \left(\mu - 1\right)\xi^2 + 3\left(\mu - 3\right)}{-\dfrac{2}{9}\mu\xi^2 + \left(\mu - 1\right)\xi} \tag{57}$$

6.2 Porosity-dependent hardening law and suffusion induced straining

The original Sinfonietta-Classica model assumes the following hardening law that links the variation of the preconsolidation pressure to the plastic strain rate :

$$\dot{p}_c = \frac{p_c}{\beta_p}\left(-\dot{\varepsilon}_v^p + \varkappa\sqrt{\dot{\boldsymbol{\varepsilon}}_d^p : \dot{\boldsymbol{\varepsilon}}_d^p} + \varpi\sqrt[3]{\det\dot{\boldsymbol{\varepsilon}}_d^p}\right) \tag{58}$$

This law introduces three non-dimensionnal parameters β_p, $\varkappa$ and ϖ: β_p is a logarithmic plastic compliance under isotropic loading, $\varkappa$ provides the contribution of the deviatoric part of the plastic strain rate to the hardening. Finally, ϖ takes into account the effect of the determinant of the plastic strain on the hardening. In many curcumstances the last coefficient can be assumed to vanish, as we will do from now-on.
The hardening law was formulated for a healty soil, i.e. a soil which was not subjected to any degradation (e.g. chemical dissolution, internal erosion, grain crushing) involving porosity changes. In this specific case, the grain incompressibility condition expressed in terms of the rate of irreversible changes reads as: $\dot{\varepsilon}_v^p = \dot{\phi}^p$. Taking into account this result, we interpret the first term on the right hand side of the hardening law (58) as the irreversible changes in the porosity and we reformulate the hardening law in terms of ϕ^p. According to equation (37) the increment of the preconsolidation pressure reads as:

$$\dot{p}_c = \frac{p_c}{\beta_p}\left(-\dot{\phi}^p + \varkappa\dot{\bar{\epsilon}}^p\right) \tag{59}$$

This alternative formulation clearly underlines the constitutive relation between the preconsolidation pressure and the variation of irreversible porosity and it consequently naturally allows to introduce the effect of porosity changes due to suffusion. Consider the rate form of the grain incompressibility condition

$\dot{\phi}^p = \dot{\phi}^{er} + \dot{\varepsilon}_v^p$, the hardening law becomes:

$$\dot{p}_c = \frac{p_c}{\beta_p}\left(-\dot{\phi}^{er} - \dot{\varepsilon}_v^p + \varkappa\dot{\bar{\epsilon}}^p\right) \tag{60}$$

Equation (60) now accounts for the reduction of the preconsolidation pressure during suffusion. The consequences of the above formula are not trivial: the loading surface $\partial\mathbb{S}$ tends to shrink towards the stress state in the occurence of suffusion.
The hardening law expressed in terms of ϕ^p allows to integrate the expression of the preconsolidation pressure p_c.

6.3 Implication of the porosity-dependent hardening law

The implications of the envisaged porosity-dependent model can be better understood by performing a thought experiment. Consider a granular sample on which a given effective stress $\boldsymbol{\sigma}'$ is applied such that $f(\boldsymbol{\sigma}', p_{c0}) < 0$, p_{c0} being the initial value of the preconsolidation pressure. The mechanical response of the soil is therefore fully elastic. Consider now the case that a suffusive process takes place, the preconsolidation pressure decreases from p_{c0} until the loading surface reaches the stress state. During the decrease of p_c, the increase of ϕ^{er} is not accompanied by changes in the plastic strain, nevertheless, eventual changes in the total strain may be involved because of the variations of the elastic strain induced by the dependency of the stiffness tensor $\mathbb{C}$ on ϕ^{er}. Once the shrinking loading surface has reached the constant stress $\boldsymbol{\sigma}'$: $f(\boldsymbol{\sigma}', p_c) = 0$, the preconsolidation pressure can no longer decrease since the effective stress state must remain plastically admissible. Then in order to counterbalance the increase of ϕ^{er}, the plastic strain must evolve to hold the condition $\dot{p}_c = 0$ true. The condition $\dot{p}_c = 0$ hence implies a relation between the components of the plastic strain rate and $\dot{\phi}^{er}$:

$$\dot{\phi}^{er} + \dot{\varepsilon}_v^p = \varkappa\dot{\bar{\epsilon}}^p \tag{61}$$

As a consequence of equation (61), we notice that during suffusive processes both the spherical and deviatoric parts of the plastic strain tensor evolve. This evolution is governed by the current stress state due to the flow rule (54).
Consider now a dense granular sample that we want to test under drained triaxial conditions. The pre-suffusion behaviour should be similar to that of a dense sand, characterized by a peak of the deviatoric stress q. After suffusion, the sample is less dense and behaves like a loose sand exhibiting just an asymptotic tendency to the residual state when the drained triaxial test is driven by axial displacement. One may notice that at this stage of the model development, no strength reduction of the residual behaviour is introduced due to suffusion. Experimentally[17], a strength reduction is observed that concerns only the stress peak and is due to the changes on the density state, from dense to loose.
A graphic explanation of this statement is provided in Figure (**1**). Let p'_0 and p_{c0} be the value of the mean effective pressure and the preconsolidation pressure, respectively, at the begining of a drained triaxial stress and before suffusion. Figure (**1**) illustrates the maximum deviatoric stress q supported by an intact soil sample (dashed line) and by the same sample after suffusion (solid line), with respect to the confinement state p'_0/p_{c0}. Regarding the intact sample, below the value $(p'_0/p_{c0})^1$, the soil deviatoric stress envelop is above the locus of the residual strength of the soil (line (Ξ)). So, in this region, the soil behaviour is characterized by a peak of strength: the soil behaves like a dense soil. Above $(p'_0/p_{c0})^1$, i.e. the region "(2)" in Figure (**1**), the maximum deviatoric stresses envelop corresponds to the residual strengths line (Ξ): the soil behaves like a loose one. Considering the same initial confinement state (p'_0/p_{c0}), then due to suffusion, the value of $(p'_0/p_{c0})^1$ decreases, becoming $(p'_0/p_{c0})^{1'}$. Consequently, if: $(p'_0/p_{c0})^{1'} \leqslant (p'_0/p_{c0}) \leqslant (p'_0/p_{c0})^1$, the soil behaviour changes from that of a dense soil to that of a loose one during suffusion, see Figure (**1**).
We underline that for drained triaxial test without suffusion, the residual strength is reached when $\dot{p_c} = 0$,

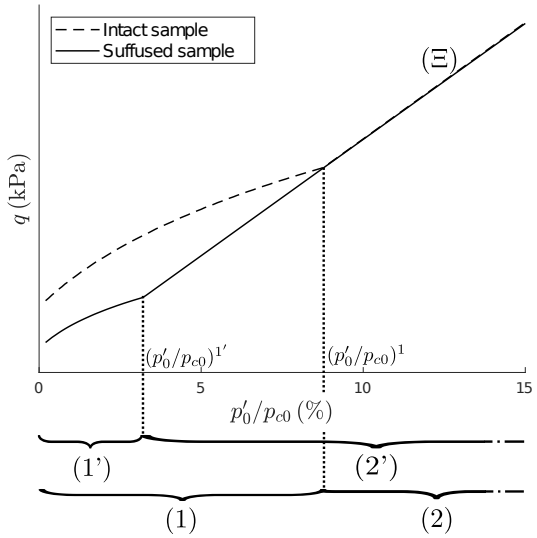

Fig. 1: Maximum stresses envelop for drained triaxial loading, for intact and suffusive soil

so the dilatancy at failure is given by:

$$\varkappa\dot{\epsilon}^p = \dot{\varepsilon}_v^p \Leftrightarrow d = -\varkappa \tag{62}$$

in such a way that ultimate stress ratio ξ verifies:

$$\frac{2}{9}\mu\xi^3 - (\mu-1)\,\xi^2 + 3\,(\mu-3) = \varkappa\left(-\frac{2}{9}\mu\xi^2 + (\mu-1)\,\xi\right) \tag{63}$$

So for a positive $\varkappa$, the residual stress state is reached above the characteristic state line. We notice that for the specific case of $\varkappa = 0$, the soil can not pass through the characteristic state line by hardening: once $\xi = Z$ is reached, volumetric plastic strain does not evolve anymore and p_c remains constant. Consequently, for such a soil, the characteristic state line and the locus of residual stress states are confused.

6.4 Porosity-driven characteristic state

We now introduce a way to model a soil initially contractive becoming dilative after a suffusion process and being subjected to a residual strenght reduction[22]. As previously said, the nature of the volumetric plastic behaviour of the soil (i.e. dilative or contractive) is fully determined by the location of the stress state with respect to the characteristic state line. From the two sides of this line, the volumetric plastic behaviour of the soil is different: if $\xi < Z$, then the soil is plastically contractive, if $\xi > Z$, then the soil is plastically dilative. The limit case $\xi = Z$, corresponds to the characteristic state line on which the soil is plastically incompressible. Moreover, for any confining pressure p', the residual strength of the soil depends on the characteristic state line slope: the higher Z, the higher the residual strength. Aiming at modelling the strength reduction induced by suffusion, we assume Z to decrease with the amount of the eroded mass, which implies the phase transition angle to be ϕ^{er}-parametrized, say $\varphi = \varphi\,(\phi^{er})$ varying from an initial value φ_{max} to a degraded one φ_{min} reached once every erodible grains is detached. To construct this dependency, we consider that during suffusion, the first group of detached particles does not take parts to the force chains so that the friction angle does not change during the early evolution of ϕ^{er}. Next, we assume that a threshold value of ϕ^{er} exists beyond which φ is strongly affected by the increase of porosity. This threshold is supposed to be proportional to the maximum of ϕ^{er} i.e. $\phi_c^{er} = A\phi_{max}^{er}$ with $0 \leqslant A \leqslant 1$. The following transition

is therefore proposed:

$$\varphi\left(\phi^{er}\right)=\frac{1}{2}\varphi_{min}\left(1+\tanh\left(\frac{1}{l}\left(\phi^{er}-A\phi_{max}^{er}\right)\right)\right)+\frac{1}{2}\varphi_{max}\left(1+\tanh\left(\frac{1}{l}\left(A\phi_{max}^{er}-\phi^{er}\right)\right)\right) \tag{64}$$

where l is a non-dimensional width factor. The higher the value of l is, the smoother the transition from φ_{max} to φ_{min} is (see Figure (**2**)). If the effective stress state is fixed, the consequence of the decrease of φ is the following: when the stress state is such that $\xi < Z\left(\varphi_{min}\right)$, then the soil is and remains contractive during suffusion. When the stress state is above the intact characteristic state line, i.e. $\xi > Z\left(\varphi_{max}\right)$, the soil is and remains dilative during suffusion. Finally, if the stress ratio belongs to the interval $\left[Z\left(\varphi_{min}\right), Z\left(\varphi_{max}\right)\right]$ then the soil is first contractive and can become dilative during suffusion if the amount of the eroded mass is sufficient. From now-on, we call this region the characteristic state zone. We recall that the present phenomenon is not interpreted as a hardening process and ϕ^{er} simply parametrizes Z.

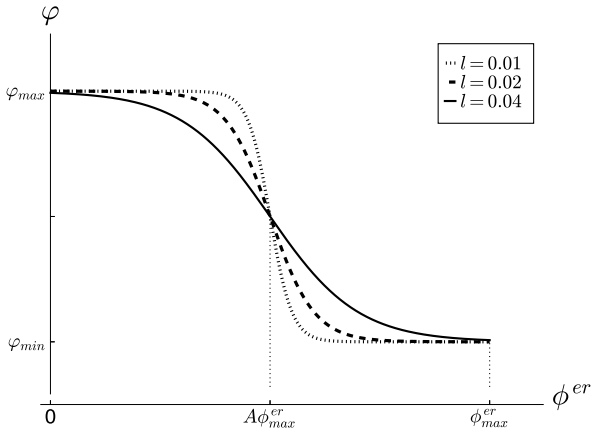

Fig. 2: Friction angle at characteristic state against suffusion induced porosity

To conclude, the porosity dependent hardening law (equation (60)) enables our model to reproduce strains variations during suffusion and the effect of the change in the density state, from dense to loose. The φ parametrization, i.e. the Z parametrization during suffusion allows to model the changes in the residual strength and governs the nature of the strain variation: purely contractive, or contractive then dilative, purely dilative. This latter parametrization is most probably strongly influenced by the grain size distribution (i.e. the initial fine content), the angularities of the grains, the direction of the seepage flow with respect to the principal stresses directions[17], and even the fabric of each soil[18]. We recall that such a parametrization depends on the soil type: some soils are subjected to characteristic state changes during suffusion, whereas other soils are not. For the latter type of soils, the amount of eroded fines does not affect the mobilized friction, so the friction angle φ does not change during suffusion. To model it, the hypothesis $\varphi_{max}=\varphi_{min}$ holds.

7 Numerical results

The aim of this section is to illustrate the abilities of the developed elasto-plastic model to qualitatively reproduce the mechanical behaviour of a suffusive soil before, during and after suffusion, at the scale of a material point. Two loading conditions are considered: drained triaxial conditions and oedometric conditions. In what follows, we do not consider how the suffusion induced porosity evolves with respect to time due to the hydraulic gradient and we limit our attention on a quasi-static evolution driven by suffusion, say on a quasi-static irreversible process where the applied loading is parametrised by ϕ^{er}. Since the present

study is devoted to expose the response of the elasto-plastic model we do not take into account the damage effect introduced in section 5.1 and the elastic stiffness tensor $\mathbb{C}$ is assumed constant during the suffusion process.

7.1 Drained triaxial test

With the aim of validating the model versus experimental results[17, 22], we simulated a series of drained triaxial loading paths during which suffusion occurs at different levels of stress. Each loading paths is separated into three steps: (i) an initial mechanical loading path, driven by the applied axial strain, ending at a fixed value of the stress ratio ξ_i; (ii) a suffusion induced porosity variation at constant stress state driven by ϕ^{er} which ranges between 0 and ϕ^{er}_{max}; (iii) another strain driven loading path, until the strength of the soil is mobilized. The sets of material parameters are choosen in order to reproduce qualitatively the results from the aforementioned experimental studies.
Several simulations are carried out for different levels of stress ratios ξ_i at the begining of the suffusion process, in particular the left and the right panels of Figure **3** are relative to the case of initially dense and initially loose erodible soils, respectively. Following experimental references in the case of a dense sample[17], three differents loading paths have been considered, during which ξ_i is equal to of 0, 1.2 and 1.5. Moreover, regarding the experimental results provided, we assume that for this material, the variations of residual strength during suffusion is not the predominent effect, the parametrization of the friction angle by ϕ^{er} is therefore not taken into account assuming $\varphi_{min} = \varphi_{max}$. For the loose sample, only one test is carried out, during this path, $\xi_i = 0$ as in experimental references[22]. Also in this case, the set of material parameters are deduced also from this experimental study, see Table 1. First we focus on the response of the dense

Table 1: Material parameters for the tested samples under drained triaxial conditons

Sand type	E (MPa)	ν	β	φ_{max} (deg)	φ_{min} (deg)	A	l	β_p	$\varkappa$	p_{c0} (kPa)	ϕ^{er}_{max}
Dense sand	4.34	0.36	1.2	41	41	-	-	0.012	0	720	0.031
Loose sand	3.46	0.25	1.2	38.5	36	0.5	0.01	0.01	0	50	0.05

sample. Regarding Figure (**3**a) and (**3**c), we observe that the intact sample shows a peak strength reached during a purely elastic phase (see Figure (**3**c)). In fact, the initial confinement p'_0 is substantially lower than the value of p_{c0}, then, during the first step of the loading path (mechanical loading) the loading surface is reached for a soil stress state slightly larger than that corresponding to the characteristic state. Once the loading surface is reached, plastic strains occur, and the dilative character of the latter induces a softening of the soil, explaining the post-peak behaviour. The maximum strength of the dense sample is reduced during suffusion: as exposed in subsection 6.2, the peak strength decreases to a lower value, and for a sufficiently large porosity change induced by suffusion, it attains the residual strength. This means that even if the soil shows a lower maximum strength after suffusion, the ultimate mobilizable strength remains the same, characterized by $\xi = Z$ (due to $\varkappa = 0$). The transition from the dense to the loose state is also observable in terms of volumetric strains, see Figure (**3**e). As previously said, for the dense soil the maximum strength is located above the characteristic state line and once the peak reached, the stress ratio decreases toward the residual strenght. This softening behaviour is acompagnied by volumetric dilation so that the total volumetric strain ε_v increase once the strength peak reached. Once the soil eroded, no softening occurs and the strength increases until the residual strength is reached, which corresponds to volumetric contraction: the total volumetric strain ε_v decreases until the condition of non-dilatancy is attained (i.e. $\xi = Z$). As a matter of fact, since for this sample $\varkappa = 0$, the stress ratio can not overwhelm the characteristic state line through hardening and the volumetric strains remains constant once $\xi = Z$. Moreover, from Figure (**3**e),

it can be observed that for the same axial strain level and until the characteristic state is not reached, a soil suffused at a lower ξ_i will present a larger volumetric strain than a soil suffused at a higher ξ_i. This phenomenon is directly linked to the shrinkage of the loading surface: since p_c decreases because of suffusion, the initially elastic material becomes elasto-plastic and hardening of the material is now required to increase the axial strain during the post-suffusion mechanical loading. The more p_c decreases, the more the hardening needed is important. In order to fulfill this requirement, plastic contraction increases strongly during the post-suffusion loading and so the total volumetric contraction.
Now we focus on the loose sample. This soil exhibits a hardening elasto-plastic behaviour and the ultime strength is the residual one, characterized by $\xi = Z$ due to $\varkappa = 0$. In this case we parametrize the characteristic state line slope with ϕ^{er} (see equation (64)), the value of the stress ratio at failure therefore decreases during suffusion (see Figure (**3**b) and (**3**d)). From Figure (**3**d) we observe that at the same stress level, the eroded sample exhibits a larger axial strain and a slightly lower tangent stiffness. Even if the residual strength is decreased, the stress-strain behaviour of the soil sample does not change: it was initially that of a loose sample, and it remains like this after suffusion. As a matter of fact, regarding Figure (**3**f), the volumetric behaviour does not change significatively and the difference between the volumetric strains of the suffused and intact samples is mainly due to the volumetric strain developed during the suffusion.
Comparing the obtained results with the experiments retrieved from the literature one can conclude that the model is capable to reproduce two types of suffusive behaviours: (*i*) the transition from a dense behavior to a loose one, characterized by the disappearance of the peak strength and by a highly contractive post-suffusion behaviour; (*ii*) the reduction of the residual strength of an initially loose sample, without a radical change in the behaviour type regarding the volumetric strains and tangent stiffness. For natural soils which may be of a different grading from the gap-graded soils modeled in this work, these effects can occur simultaneously. One can notice that the straight parts of the loading surfaces (for low stress levels) correspond in fact to the tension cut-off existing in the Sinfonietta-Classica model[32]

7.2 Oedometric test

In this section we simulate the behaviour of a suffusive soil under oedometric conditions. The set of material parameters is based on the one used to model loose sand under drained conditions (see Table 1, line 2). The only difference being that we do not longer take into account the decrease of the friction angle due to suffusion: $\varphi_{min} = \varphi_{max} = 38.5°$. Starting from an initial state of stress defined by $\xi = 0$ and $p'_0 = 0.2p_{c0}$, we apply on the intact soil a mechanical loading as a vertical strain increment $\dot{\varepsilon}_a$ with locked lateral strain, say in axisymmetric conditions:

$$\varepsilon_L = \varepsilon_2 = \varepsilon_3 = 0 \tag{65}$$

Then, we start to erode the specimen from different values of ξ, considering ϕ^{er} as an incremental loading from 0 to ϕ^{er}_{max}, with a constant vertical stress σ_a. Once the suffusion is achieved, we reload the material with vertical strain increments, always keeping fixed the oedometric conditions. The aim of these simulations is double: (*i*) to determine if the suffusion affects the current stress-strain state of the soil (*ii*) to evaluate the effects of suffusion over the post-suffusion response. The results of the simulations are plotted into Figure (**4**), in which Figure (**4**b) is the zoom of the box plotted in Figure (**4**a). Let us analyse the obtained stress paths during suffusion. The stress evolution follows different paths: (*i*) for low levels of stress at the beginning of suffusion, the isotropic pressure p' decreases and the deviatoric stress q increases (i.e. ξ increases) (*ii*) for high levels of stress at the beginning of suffusion, the inverse phenomenon occurs, p' increases and q decreases (i.e. ξ decreases). We can explain this phenomenon by within the framework of soil degradation using a similar argument as that developed to explain calcarenite degradation due to chemical attacks[35]. Consider the expression of the dilatancy given by equation (57) and restrict attention to the kinematics of the oedometric test. As already mentioned, during an oedometric test, the lateral

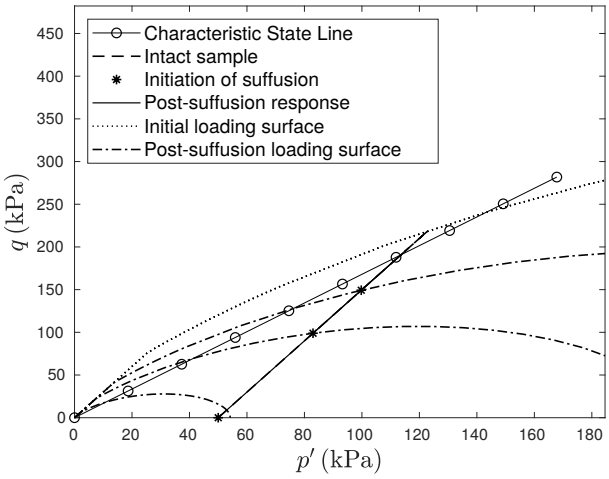

(a) Effective stress paths in the Cambridge plane (dense)

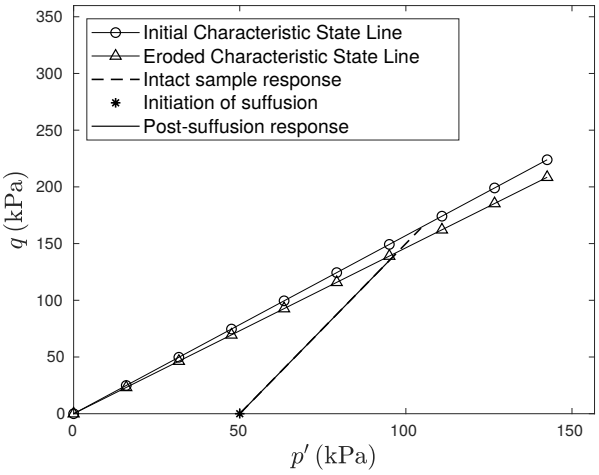

(b) Effective stress paths in the Cambridge plane (loose)

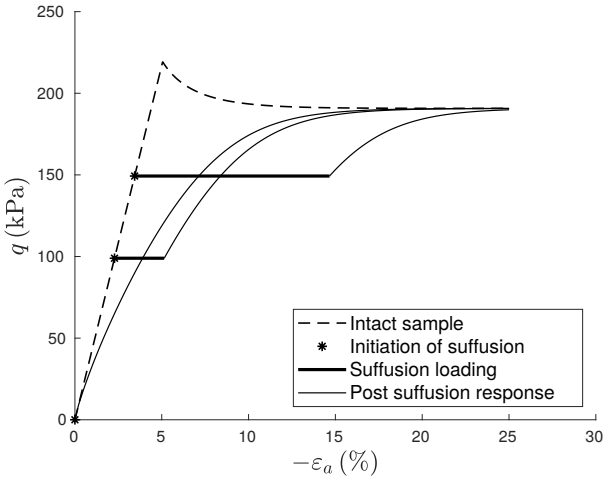

(c) Deviatoric stress against axial strain (dense)

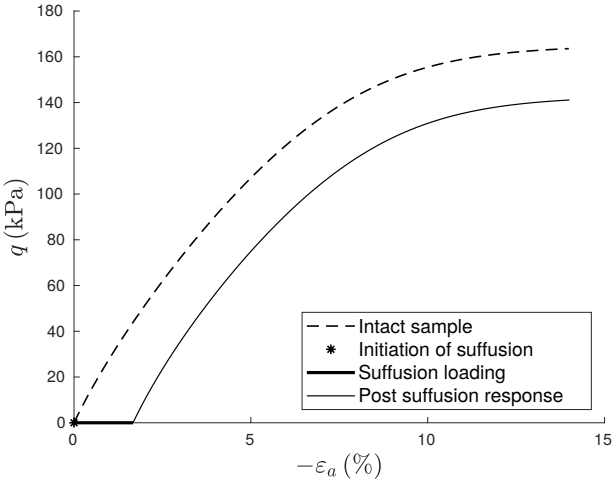

(d) Deviatoric stress against axial strain (loose)

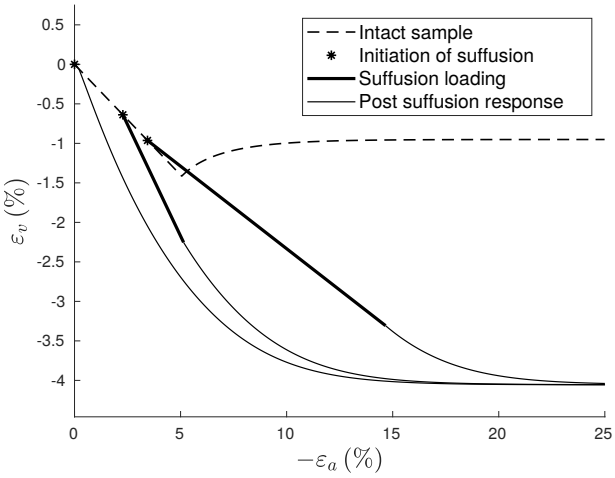

(e) Volumetric strain against axial strain (dense)

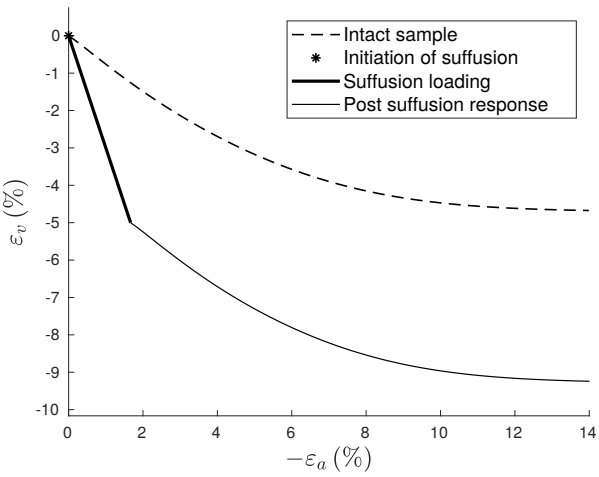

(f) Volumetric strain against axial strain (loose)

Fig. 3: Dense and loose suffusive soils compared to intact sample - drained axisymmetric triaxial conditons

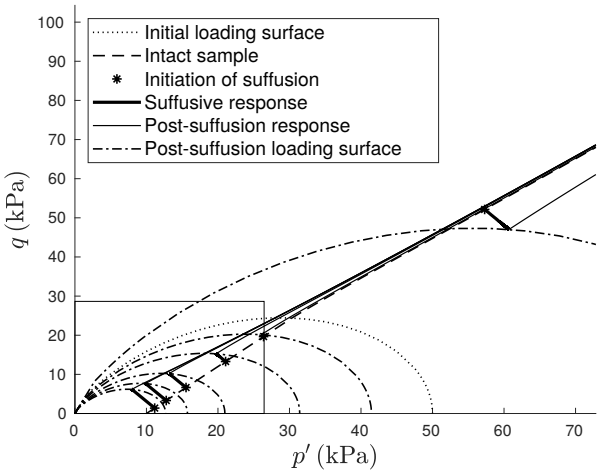

(a) Effective stress paths in the Cambridge plane

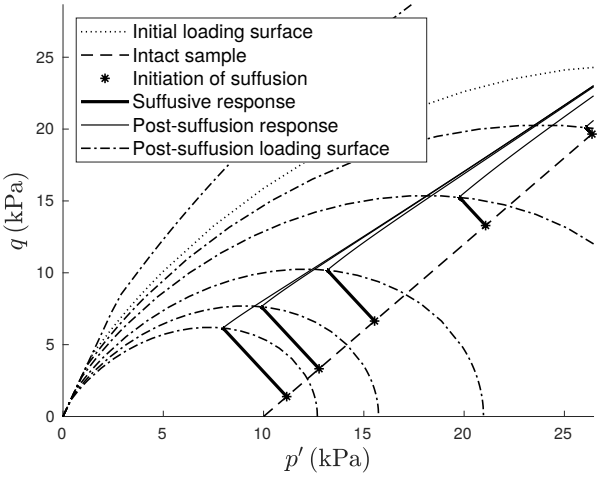

(b) Effective stress paths (zoom on low stress levels)

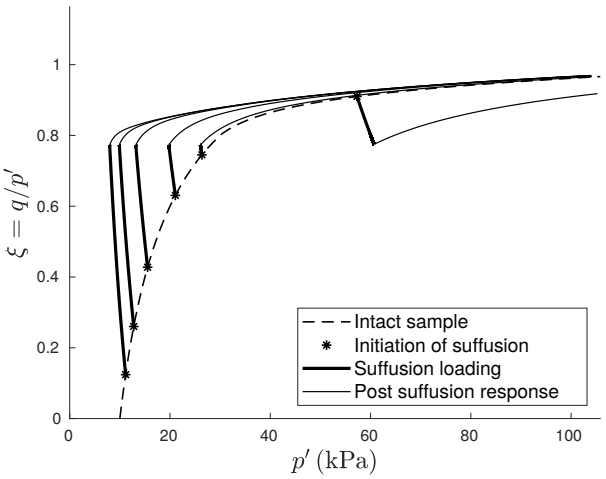

(c) Evolution of the stress ratio along the loading paths

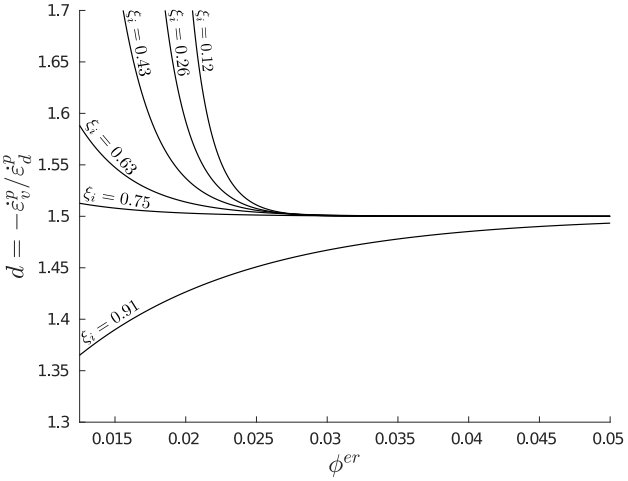

(d) Evolution of dilatancy during suffusion

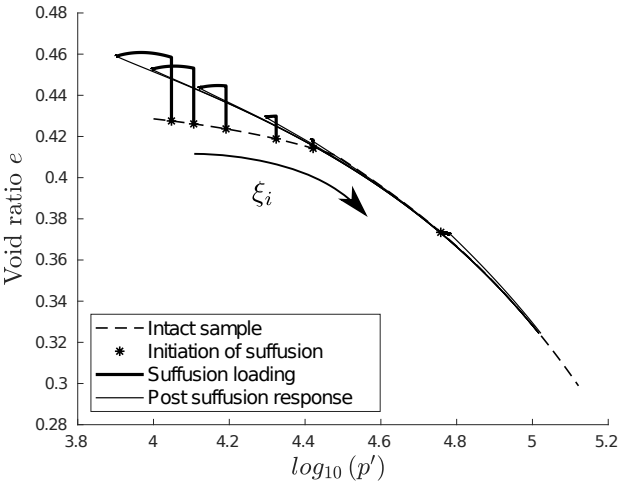

(e) Evolutions of the void index along the loading paths

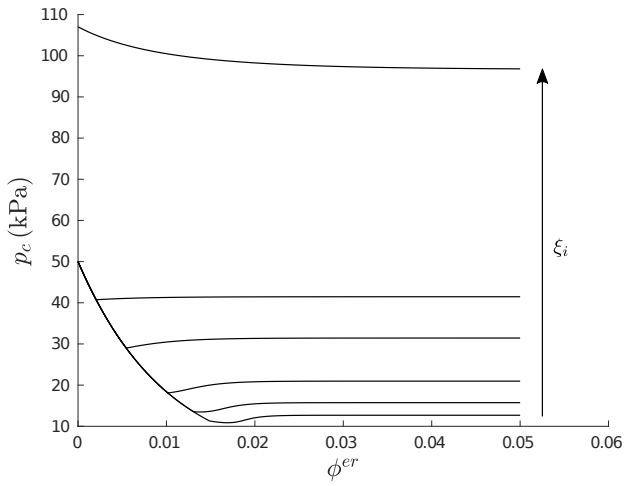

(f) Evolutions of preconsolidation pressure during suffusive loadings

Fig. 4: Suffusive soil compared to intact sample - oedometric conditions

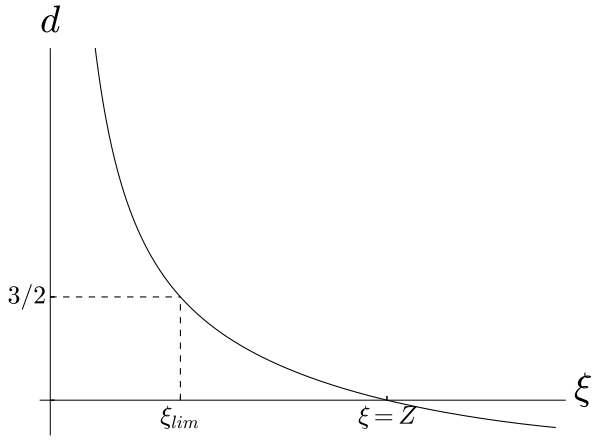

Fig. 5: Dilatancy against stress ratio for axisymmetric conditions

strains are inhibited, then:

$$\dot{\varepsilon}_L = 0 \Leftrightarrow \dot{\varepsilon}_L^p = -\dot{\varepsilon}_L^e \tag{66}$$

For a sufficiently large suffusion induced porosity variation, the soil tends to reach an equilibrium at which the stress state does not evolve anymore during suffusion. This implies the zero of the elastic strain rate. Then the axial plastic strain rate is equal to the total axial strain rate, and from the previous relationship we get:

$$\dot{\varepsilon}_L^p = 0 \quad \text{and} \quad \dot{\varepsilon}_a^p = \dot{\varepsilon}_a \tag{67}$$

So the volumetric and deviatoric plastic strain rates are given by:

$$\dot{\varepsilon}_v^p = \dot{\varepsilon}_a \quad \text{and} \quad \dot{\varepsilon}_d^p = \frac{2}{3}\left|\dot{\varepsilon}_a^p - \dot{\varepsilon}_L^p\right| = \frac{2}{3}\left|\dot{\varepsilon}_a\right| \tag{68}$$

As a consequence, the dilatancy d (see equation (56)) tends to 3/2 during suffusion, see Figure (**4**d). Due to the axisymmetric conditions of the oedometric test, we get from equation (57) the asymptotic value of ξ_{lim} towards which ξ asymptotically tends during suffusion. Since in axisymmetric conditions d is a continuous and monotonically decreasing function of ξ, the evolution of ξ during suffusion depends on the stress ratio at suffusion initiation ξ_i with respect to ξ_{lim}. If ξ_i is above ξ_{lim}, then the stress ratio decreases asymptotically to ξ_{lim}, conversely, if ξ_i is below ξ_{lim}, the stress ratio increases asymptotically to ξ_{lim} as shown on Figure (**5**):

$$\text{if:} \quad \xi_i < \xi_{lim} \quad \text{then:} \quad \dot{\phi}^{er} > 0 \Rightarrow \dot{\xi} > 0 \tag{69a}$$

$$\text{if:} \quad \xi_i \geqslant \xi_{lim} \quad \text{then:} \quad \dot{\phi}^{er} > 0 \Rightarrow \dot{\xi} \leqslant 0 \tag{69b}$$

These inequalities explain the evolution of q and p' during suffusion: if inequality (69a) holds true, then q increases and p' decrease; if inequality (69b) holds true, q decreases and p' increases. An illustration of this evolution law is reported in Figure (**4**c). In practice, since oedometric conditions are representative of many in-situ conditions, it appears that the stress in a soil-mass should evolves during suffusion.
In Figure (**4**e), the response of the soil is plotted in the $e - log_{10}(p')$ plan; a kind of consolidation curve is retrieved. The first evident effect of the increase of ϕ^{er} is the drastic increase in the void ratio e for sample eroded at low stress level. The second phenomenon is the decrease of the preconsolidation-pressure just due to suffusion, see Figure (**4**f). If the initial stress state is within the elastic domain, the preconsolidation pressure strongly decreases. If the initial stress state is already plastic, the preconsolidation pressure evolves slightly as plastic strains counterbalance the reduction of p_c due to the increase of ϕ_{er}. Regarding Figure (**4**f), the value of ϕ^{er} corresponding to the change of the slope of p_c versus ϕ_{er} corresponds to the value of ϕ^{er} for which the loading surface is reached by the stress state. For samples eroded at low stress ratio, we

observe a slight increase of p_c once the loading surface has reached the current mechanical state. In fact, in order to follow the characteristic stress path imposed by the kinematic contraints (equations (68),(69a)), the material needs hardening and p_c increases consequently.

8 Conclusions

In the light of the classical poromechanics, the constitutive modelling of soils subjected to suffusion has been revisited, and a new coupling between suffusion kinetics, fluid diffusion and mechanical behaviour has been proposed. As a result, the rate of suffusion induced porosity depends on the hydraulic gradient, and the mechanical state of the skeleton. An elastoplastic model accounting for the mechanical consequences of suffusion has been established by introducing the porosity induced by suffusion into an existing elasto-plastic model (the Nova Sinfonietta-Classica model). The extended model allows to reproduce the stress strain behaviour of dense and loose gap-graded soils, under monotonic drained triaxial test, coupled with suffusion. The loss of density as well as its mechanical consequences are recovered. By parametrizing the characteristic state line slope with the porosity change due to suffusion, the decrease of the residual strengh of loose suffusive soils is modelled. Moreover, the response of suffusive soil under oedometric conditions has been predicted. During suffusion, the stress state of the soils evolves, converging toward a value that enforce the dilatancy to 3/2. The numerical simulations have been performed at the scale of a material point, which is expected to be a Representative Elementary Volume. Consequently, the presented numerical results do not take into account the heterogeneity induced by suffusion in real samples and reported in the literature. To reduce this lack of representativity and model the suffusion consequences at the scale of an earth structure, further works will concentrate on the implementation of the whole model into a finite element code. Further developments will be also devoted to (*i*) the validation of the coupled model thanks to multiscale analysis and to (*ii*) the calibration of the constitutive parameters.

References

[1] Bonelli S. *Erosion of geomaterials.* John Wiley & Sons; 2012.

[2] Fell R., Fry J-J. *Internal Erosion of Dams and Their Foundations: Selected and Reviewed Papers from the Workshop on Internal Erosion and Piping of Dams and their Foundations, Aussois, France, 25–27 April 2005.* CRC Press; 2014.

[3] Lafleur J., Mlynarek J., Rollin A-L. Filtration of broadly graded cohesionless soils. *Journal of Geotechnical Engineering.* 1989;115(12):1747–1768.

[4] Marot D., Bendahmane F., Nguyen H-H. Influence of angularity of coarse fraction grains on internal erosion process. *La Houille Blanche.* 2012;(6):47–53.

[5] W. Skempton A, M. Brogan J. Experiments on piping in sandy gravels. *Geotechnique.* 1994;44:449-460.

[6] Reddi L-N., Lee I-M., Bonala M-V-S. Comparison of internal and surface erosion using flow pump tests on a sand-kaolinite mixture. *Geotechnical testing journal.* 2000;23(1):116–122.

[7] Perzlmaier S., Muckenthaler P., Koelewijn A-R. Hydraulic criteria for internal erosion in cohesionless soil. *Fell, R. and Fry, J.-J.(Eds.), Internal erosion of dams and their foundations.* 2007;:179–190.

[8] Marot D., Le V-D., Garnier J., Thorel L., Audrain P. Study of scale effect in an internal erosion mechanism: centrifuge model and energy analysis. *European Journal of Environmental and Civil Engineering.* 2012;16(1):1–19.

[9] Rochim A., Marot D., Sibille L., Le V-T. Effects of Hydraulic Loading History on Suffusion Susceptibility of Cohesionless Soils. *Journal of Geotechnical and Geoenvironmental Engineering.* 2017;143(7):04017025.

[10] Marot D., Rochim A., Nguyen H-H., Bendahmane F., Sibille L. Assessing the susceptibility of gap-graded soils to internal erosion: proposition of a new experimental methodology. *Natural Hazards.* 2016;83(1):365–388.

[11] Moffat R., Fannin R-J. A hydromechanical relation governing internal stability of cohesionless soil. *Canadian Geotechnical Journal.* 2011;48(3):413–424.

[12] Chang DS, Zhang LM. Critical hydraulic gradients of internal erosion under complex stress states. *Journal of Geotechnical and Geoenvironmental Engineering.* 2012;139(9):1454–1467.

[13] Bendahmane F., Marot D., Alexis A. Experimental parametric study of suffusion and backward erosion. *Journal of Geotechnical and Geoenvironmental Engineering.* 2008;134(1):57–67.

[14] Chen C., Zhang L-M., Chang D-S. Stress-strain behavior of granular soils subjected to internal erosion. *Journal of Geotechnical and Geoenvironmental Engineering.* 2016;142(12):06016014.

[15] Sibille L., Marot D., Sail Y. A description of internal erosion by suffusion and induced settlements on cohesionless granular matter. *Acta Geotechnica.* 2015;10(6):735–748.

[16] Sterpi D. Effects of the erosion and transport of fine particles due to seepage flow. *International Journal of Geomechanics.* 2003;3(1):111–122.

[17] Chang D-S, Zhang L-M. A stress-controlled erosion apparatus for studying internal erosion in soils. *Geotechnical Testing Journal.* 2011;34(6):579–589.

[18] Muir Wood D, Maeda K, Nukudani E. Modelling mechanical consequences of erosion. *Géotechnique.* 2010;60(6):447–457.

[19] Scholtès L., Hicher P-Y., Sibille L. Multiscale approaches to describe mechanical responses induced by particle removal in granular materials. *Comptes Rendus Mécanique.* 2010;338(10-11):627–638.

[20] Aboul Hosn R., Sibille L., Benahmed N., Chareyre B. A discrete numerical model involving partial fluid-solid coupling to describe suffusion effects in soils. *Computers and Geotechnics.* 2018;95:30–39.

[21] Hu Z., Zhang Y., Yang Z. Suffusion-induced deformation and microstructural change of granular soils: a coupled CFD–DEM study. *Acta Geotechnica.* 2019;14(3):795–814.

[22] Ke L., Takahashi A. Drained monotonic responses of suffusional cohesionless soils. *Journal of Geotechnical and Geoenvironmental Engineering.* 2015;141(8):04015033.

[23] Vardoulakis I., Stavropoulou M., Papanastasiou P. Hydro-mechanical aspects of the sand production problem. *Transport in porous media.* 1996;22(2):225–244.

[24] Stavropoulou M., Papanastasiou P., Vardoulakis I. Coupled wellbore erosion and stability analysis. *International journal for numerical and analytical methods in geomechanics.* 1998;22(9):749–769.

[25] Papamichos E., Vardoulakis I., Tronvoll J., Skjaerstein A. Volumetric sand production model and experiment. *International journal for numerical and analytical methods in geomechanics.* 2001;25(8):789–808.

[26] Vardoulakis I., Papamichos E. A continuum theory for erosion in granular media. *Actes de la journées scientifique internationale, Cermes.* 2001;21:41–60.

[27] Papamichos E., Vardoulakis I. Sand erosion with a porosity diffusion law. *Computers and Geotechnics.* 2005;32(1):47–58.

[28] Papamichos E. Erosion and multiphase flow in porous media. *European Journal of Environmental and Civil Engineering.* 2010;14(8-9):1129-1154.

[29] Bonelli S., Marot D. Micromechanical modelling of internal erosion. *European Journal of Environmental and Civil Engineering.* 2011;15(8):1207-1224.

[30] Zhang X-S., Wong H., Leo C-J, et al. A thermodynamics-based model on the internal erosion of earth structures. *Geotechnical and Geological Engineering.* 2013;31(2):479–492.

[31] Coussy O. *Poromechanics.* Wiley; 2004.

[32] Nova R. Sinfonietta classica: an exercise on classical soil modelling. *Constitutive Equations for Granular non-cohesive soils.* 1988;:501–519.

[33] Gurtin M-E. *An introduction to continuum mechanics.* Academic press; 1982.

[34] Simo J-C., Hughes T-J-R. *Computational inelasticity.* Springer Science & Business Media; 2006.

[35] Castellanza R., Nova R. Oedometric tests on artificially weathered carbonatic soft rocks. *Journal of geotechnical and geoenvironmental engineering.* 2004;130(7):728–739.